HL3.1: Microstructure analysis (before and) after permeation experiments: Zuidwending cavern field

Version 240409

9 April 2024

Authors

5.1.2.e

With contribution by 5.1.2.e

MaP Microstructures and Pores GmbH

Reviewed by:

5.1.2.e

[3]Brouard Consulting

[4]smartTectonics

Contents

Comment by Joyce Schmatz, March 2024

The completion of this work involved a close partnership between MaP and Geostructures. Unfortunately, Prof. Dr. Janos L. Urai passed away on May 28, 2023, while the ongoing experimental work discussed in this report was still in progress. A significant portion of the microstructure interpretation relies on conversations we had with Janos, and I want to express my gratitude for his substantial contribution to this research.

Zuidwending Workpackage 3.1: Comment by Joyce Schmatz, March 2024

The completion of this work involved a close partnership between MaP and Geostructures. Unfortunately, Prof. Dr. Janos L. Urai passed away on May 28, 2023, while the ongoing experimental work discussed in this report was still in progress. A significant portion of the microstructure interpretation relies on conversations we had with Janos, and I want to express my gratitude for his substantial contribution to this research.

Summary

This study investigates the micro-scale process of permeation behaviour. Permeation in salt rocks, also known as salt permeability, refers to the ability of fluids (such as water, hydrocarbons, or gases) to flow through the pore spaces and fractures within salt formations. Salt rocks, also called evaporites, are composed primarily of minerals such as halite (rock salt) and gypsum, and they often possess unique properties that influence their permeability behaviour. The phenomenon of permeation plays a crucial role in controlling cavern pressure development after cavern abandonment, primarily due to thermal effects and continued cavern convergence. Understanding permeation is essential for accurate simulation of cavern pressure evolution. Uncertainties persist regarding the most suitable permeation model for upscaling from grain-size to field scales. The investigation focuses on micro-structural analyses of laboratory permeation tests conducted on heterogeneous natural rock salt samples. These tests were designed to assess hydraulic properties under varying effective stresses, emphasizing the impact of anhydrite inclusions and mega-grains on fluid flow within the salt matrix. Utilizing a radial flow geometry within a standard triaxial apparatus, experiments were conducted over 30-50 days using saturated brine as the fluid medium while applying a differential stress of 1 MPa. Microstructural analysis integrated micro-CT, optical microscopy, and SEM techniques, providing insights into the intricate pore networks and internal structure of rock salt. Findings highlight preferred permeation pathways such as the interfaces of halite mega-grains with matrix grains and/or with thin anhydrite bands, which can be the dominating pathway compared to also present dilatant matrix-halite grain boundary networks. These results offer valuable insights into permeation behaviour of rock salt, particularly under saturated brine conditions, contributing to a deeper understanding of cavern pressure dynamics and improving future modelling efforts.

Zuidwending Workpackage 3.1: Comment by Joyce Schmatz, March 2024

The completion of this work involved a close partnership between MaP and Geostructures. Unfortunately, Prof. Dr. Janos L. Urai passed away on May 28, 2023, while the ongoing experimental work discussed in this report was still in progress. A significant portion of the microstructure interpretation relies on conversations we had with Janos, and I want to express my gratitude for his substantial contribution to this research.

1 Introduction

Permeation behaviour is one of the dominant factors controlling the long-term cavern pressure after abandonment of salt caverns. While the effect can be implemented in numerical codes simulating cavern pressure evolution, such models are only reliable if the underlying assumptions on the microphysical processes governing permeation are correct. To date, there is no consensus on what permeation model is best to upscale permeation from grain-size to field scales, or whether permeation is distributed or localized to some extent. Moreover, even on the grain-size scale complicating factors may arise in the form of variability in the grain size content (e.g., presence of mega-grains). Furthermore, flow along and/or through microporous impurities could play a role.

The objective of this work was to gain better understanding of prevailing permeation processes by means of microstructural investigation of laboratory permeation tests conducted on heterogeneous natural rock salt samples. The permeation tests are aimed to assess the hydraulic properties as a function of the effective stress, with a specific emphasis on the influence of anhydrite inclusions and mega-grains on fluid flow within the salt matrix.

We aimed to test the following hypothesis on the permeation mechanisms:

1. Permeation along (micro-cracked) matrix halite grain boundary network
2. Permeation through transgranular micro-cracks of the mega-grains
3. Permeation along the interface of matrix halite with halite mega-grains and/or anhydrite bands
4. Permeation through porous anhydrite

Permeation tests were performed with a radial flow geometry similar to Popp et al. (2015) over the period of 30-50 days per experiment. To allow for dissolution and precipitation effects the experiments were conducted using saturated brine as fluid medium. Moreover, the samples were subjected to a relatively low differential stress of 1 MPa. Following an initial consolidation phase, fluid pressure was gradually increased until a rapid increase of the flow was detected. Flow was initiated from a mini-cavern placed in the radial center of the cylindric sample at preselected axial depth. The location of the mini-cavern within the sample was selected based on microstructural features (density contrast) that were revealed by micro-computed tomography (Micro-CT) prior to testing.

Microstructural analysis consisted of a comprehensive multi-faceted approach, integrating micro-CT, optical microscopy, and scanning electron microscopy (SEM). Micro-CT provided three-dimensional imaging capabilities, offering insights into the internal structure and pore network of the rock salt. Optical microscopy together with SEM complemented these findings by delivering high-resolution two-dimensional images, facilitating detailed observation of micro-to nano-scale features. The combination of these techniques enabled a comprehensive understanding of the intricate microstructural characteristics affecting fluid flow within the heterogeneous rock salt material.

The following section outlines the materials and methods used, providing an outline of the experimental design and setup (for more detail please see the IfG report). Subsequently, the results of microstructural analyses from each permeation experiment are detailed chronologically. Additional images are included in the accompanying appendix. The concluding section presents the findings and recommendations. This assessment also offers a detailed examination of the grain boundary structure and potential microstructural alterations resulting from the permeation process.

2 Material and methods

2.1 Permeation experiments

Experiments were aimed to test the predicted effects of dilatancy by fluid-assisted microcracking and grain boundary dissolution-precipitation processes on permeation of Zuidwending salt around the caverns during operation and abandonment. The design of permeation experiment was discussed intensively with IfG to define a materials science-based protocol for experiments which include permeation by saturated brine, in samples under a small deviatoric (total) stress to simulate the surroundings of an abandoned cavern (reasonable values for the stress state were derived from the modelling in this project). Focus was initially on the effect of heterogeneity on permeation, the evolution of fluid pressure and rate of permeation, to characterize the dilatancy and change in grain boundary processes (dilatancy, recrystallization, re-sealing and pressure solution) during the permeation experiments.

Selected Zuidwending sub-cores were micro-cored, tubing was placed and fixed with epoxy and subsequently drilled out until approximately 1 cm below the tubing to create a mini-cavern at IfG (Figure 1). In a next step, the sample was placed in the permeation apparatus and after a hydrostatic/consolidation phase, to heal the sample, subjected to increased fluid pressure in the mini-caverns which was increased in a stepwise fashion under anisotropic stress conditions using brine (at 45 - 40 °C). In and outflow was monitored during the experiment and fluid pressure steps were increased accordingly until breakthrough was reached (for more details, see the report from IfG).

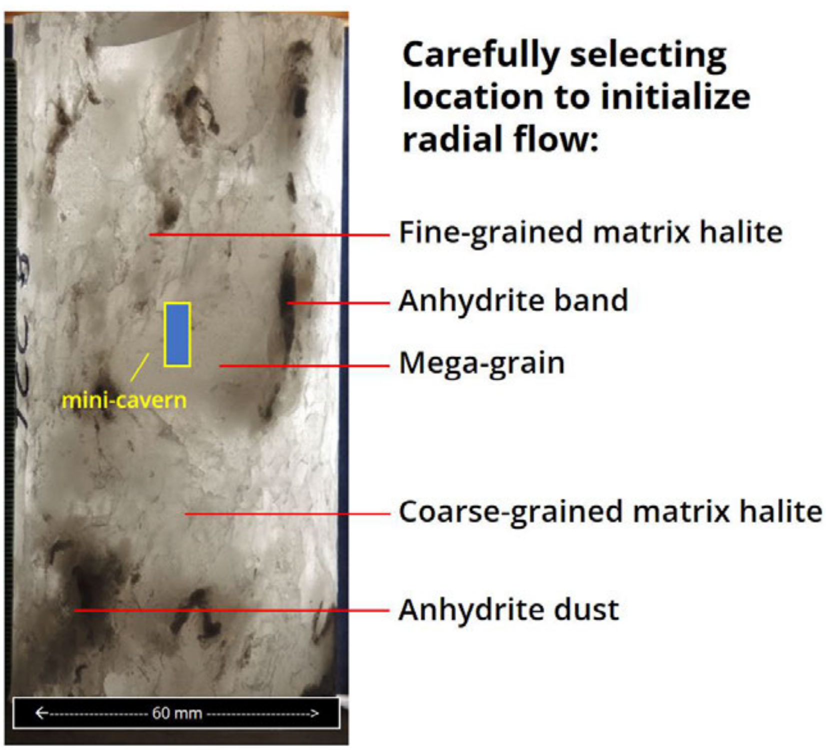

Figure 1: Generic example showing selection of location for preparation of the mini-cavern in heterogeneous rock salt.

2.2 Sample material and preparation

Sample selection of heterogeneous salt aimed to test the hypothesis on the permeation behaviour as stated above. Accordingly, samples were selected to allow testing of the different hypothesis by placing the mini-cavern at distinct locations within the core piece (Figure 1 refer to ZW3.1 CT report). The initial samples were selected based on the work presented in ZW1.1 and cut into core pieces of at least 20 centimetres long, then shipped to IfG (Table 1). Finally, based on the results from the micro-CT analysis on the initial core pieces (refer to Appendix), six samples were selected for testing at IfG.

Table 1 lists the executed IfG experiment ID (PermX), in this report the permeated samples will be named by combining the cavern field and the numbering of the IfG experiments: e.g., ZW_Perm4. See the Appendix for photographs of the selected cores prior to shipment to IfG.

Table 1. Initial core piece selection with MaP and IfG-ID of the permeation experiments

Well_Core_name	Top depth	MaP_ID core piece	Voxel size for MicroCT (µm) before and after permeation	IfG_ID permeation test	purpose
ZW A1A_2_2_452.62	453.20	ZW A1A_2_2_453.2_D	67.26/77	ZW_Perm2	Hyphothesis 1
ZW A1A_4_7_959.2	959.70	ZW A1A_4_7_959.7_D	67.26	CT-scanned before permeation	Not selected for permeation
ZW A1A_9_1_1518	1518.10	ZW A1A_9_1_1518.1_P	67.26/77	ZW_Perm1	Hyphothesis 1
ZW A2A_8_7_1505.8	1506.10	ZW A2A_8_7_1506.1_Mine	67.26/74.48	ZW_Perm3	Hyphothesis 2
ZW A3A_1_2_591.9	592.20	ZW A3A_1_2_592.2_P	67.26/74	ZW_Perm4	Hyphothesis 3&4
ZW A3A_2_1_991	991.10	ZW A3A_2_1_991.1_P	67.26/74.48	ZW_Perm5	Hyphothesis 3&4
ZW A3A_6_5_1444.5	1445.10	ZW A3A_6_5_1445.1_P	67.26/41.15	ZW_Perm6	Hyphothesis 1
ZW A4A_5_10_1028	1028.70	ZW A4A_5_10_1028.7_D	67.26	CT-scanned before permeation	Not selected for permeation

At IfG the core pieces were cored again, down to a diameter of 60mm to fit the permeation apparatus. See the **Fehler! Verweisquelle konnte nicht gefunden werden.** for exemplary photographs of the sub-cores and selection and positioning of the inner tube as discussed with IfG and Nobian. After the experiments the samples were shipped in wet and packed conditions to MaP for the MicroCT scanning and further microstructural analyses. After the CT scanning, the interior was impregnated with blue dyed epoxy under vacuum using the existing tubing to highlight the flow paths for most of the permeated samples, and the outside was stabilized with normal epoxy before cutting the permeated core pieces.

2.3 MicroCT and image processing

All permeated samples were scanned in 3D with micro-CT using a Nikon METRIS 3 X-TEK XT H 320 LC scanner. The voxel resolution is governed by the sample size, roughly 1/1000 of the field of view, resulting in a voxel size of ranging from 41-77 µm.

Several post-processing steps were required to visualize the features of interest (before and after permeation), and these steps were performed in a systematic way in order to compare scans with each other. The raw imagery consisted of 32-bit float data and was provided as .vol file format. The data was imported in Fiji (https://imagej.net/software/fiji/) for further image processing according to the dimensions and voxel size listed in (Table 1) 32-bit Real, Little-endian byte order). In a first step the data was cropped to the sample volume, excluding the steel plates to decrease the file size. Subsequently, if the data contained a significant radial gradient, it was determined and subtracted from the original data by a mathematical operation. In a next step we enhance the contrast to improve the identification of fractures, and the anhydrite. Finally, we segmented the tubing, the mini-cavern, the fractures and the anhydrite using 3D filter, local thresholding and removal of small unoriented noises to determine their fractions and to visualize the interaction between these. From the segmented fractures the fraction and the fraction of anhydrite was determined.

2.4 Microstructural analyses

The sample material was prepared for further microstructural analysis by cutting the resin-impregnated sample cylinders, coloured blue, in half parallel to the long axis. Subsequently, they were prepared and examined according to the following strategy:

High-resolution flatbed scans in transmitted light were used to study the overall microstructure of the cut faces of the samples and the thin-sections. The pixel size of these scans was 5.3 micrometers. They were also used to select sub-samples for Optical Microscopy and Scanning Electron Microscopy (SEM) imaging. Optical Microscopy was conducted in reflected and transmitted light using a Zeiss Axioscan 7 microscope equipped with an xy-scanning stage. We used the 2.5x, 5x, and 10x objectives, producing micrographs with pixel sizes of 3.45 µm, 1.38 µm, and 0.69 µm, respectively. Single images and stitched mosaics were acquired for further qualitative and semi-quantitative microstructural analyses. Hue values of the transmitted light flatbed scan images, as well as micrographs acquired using the optical microscope, were modified to allow better differentiation of the blue resin used for ex-situ visualization of the flow paths from the resin used for thin section preparation. As a result, the blue resin appears with magenta colour in the micrographs, while the resin used for thin section preparation appears greenish. Sub-samples, such as BIB polished cross-sections and thin-sections, were imaged in a Zeiss - Supra 55 field emission Scanning Electron Microscope. The reader is referred to the ZW1.2 report for further details on the methodology. Simultaneously acquired EDS was used to trace resin inside the pore space in order to visualize the preserved permeation pathways.

3 Results

The results are presented sample by sample in numerical order of the permeation experiments. The image data results include the core photographs with sample origin, Micro-CT data, flatbed scans of sections, optical microscopy of (thin) sections and SEM scans of sections and sub-samples of special interest. Essential images and descriptions are presented below. All other image data (with segmentations or annotations) are presented in the Appendix in numerical order of the permeation experiments.

3.1 ZW_Perm1

The initial sample chosen for the permeation experiment originates from a depth of 1518 meters within well ZW_A1A, specifically from core number 9 and box slab number 1. It predominantly comprises a polycrystalline halite matrix ranging from fine- to coarse-grained, mixed with irregularly dispersed anhydrite inclusions that are visible as isolated small nodules or thin layers. Additionally, minor halite mega-grains are observable within the selected core segment. The tubing was centrally positioned within the core segment (Figure 2).

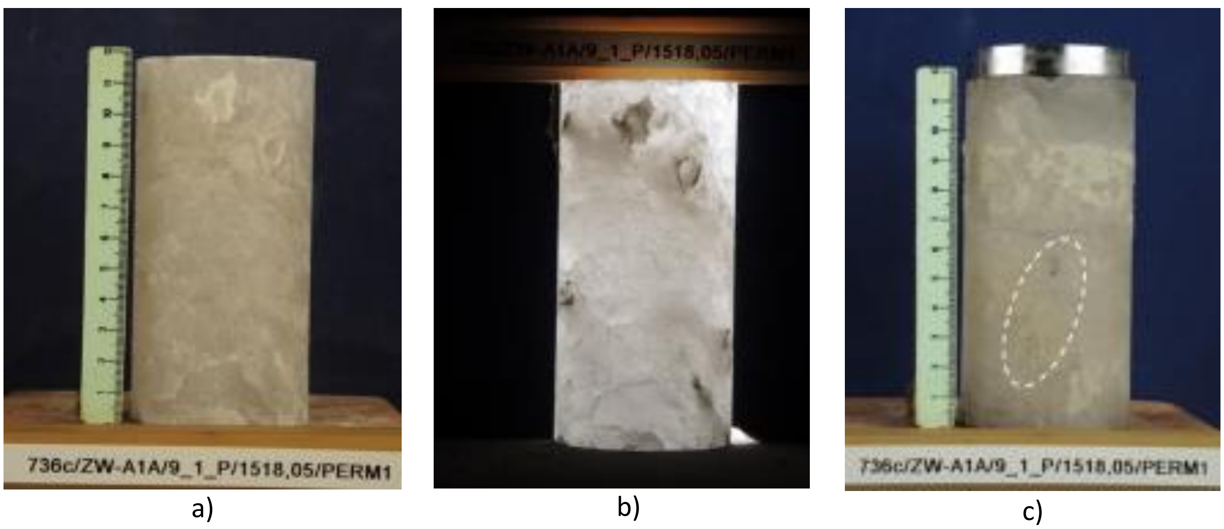

Figure 2: Photos of ZW_Perm1 showing before the permeation experiment at ambient light conditions (a). Before at transmitted lightning conditions (b) and after the permeation experiment (c) at ambient light conditions (pictures from IfG).

3.1.1 Micro-CT investigations

A Micro-CT scan was conducted both before and after the permeation experiment ZW_Perm1, as well as for all other five selected samples. The Micro-CT data before the permeation showed a homogeneous matrix, relatively fine-grained with anhydrite dust. During the experiment the brine infection rate increased rapidly after breakthrough resulting in substantial leaching and the formation of a cavern containing a kind of wormhole around the lower parts of the tubing (please refer to section 3.1.3). The micro CT data shows a fracture space of 0.53 vol% before permeation and a segmented pore space of 0.01 vol% after permeation (Figure 3:).

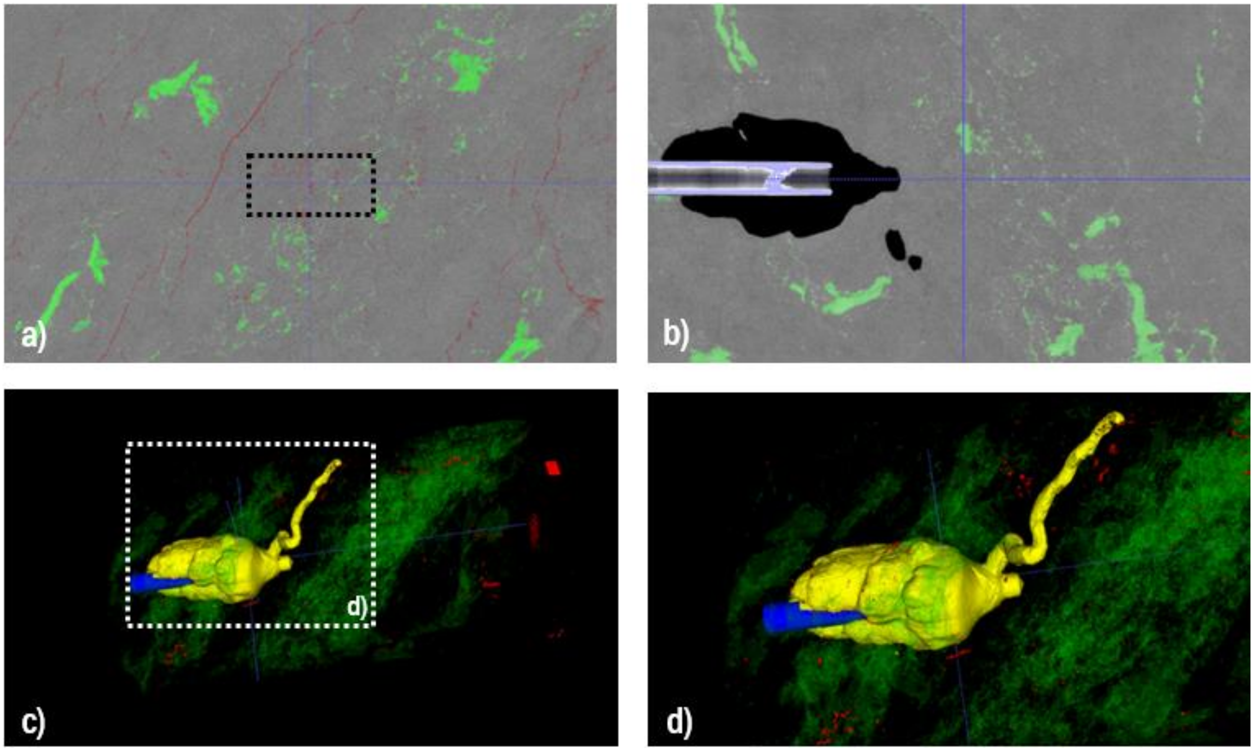

Figure 3: a) ZW_Perm1 cross-section through the Micro-CT scan before permeation, indicating the location of the tubing as well as the phase segmentation with anhydrite in green and fracture space segmented in red. b) cross-section trough Micro-CT scan after permeation, showing the phase segmentation. c) 3D visualization of segmented phases including the mini cavern indicated in yellow. d) zoomed-in 3 D visualization highlighting the mini cavern in yellow. For scaling: tube diameter is 0.6 mm.

3.1.2 Microscopy analyses

Similar to the Micro-CT analyses, the optical microscope images of the slab and thin section reveal a miniature cavity forming around the tubing (Figure 4 and Figure 5). At higher resolutions, resin impregnated matrix halite grain boundaries imply permeation along grain boundaries, though the feature appears to be localized around the mini-cavern and the wormhole. Minimal resin impregnation was observed at the grain boundaries in the thin section, with the majority of the blue-coloured epoxy concentrated along the wormhole structure due to its significant role as a dominant pathway for the fluids. As we cannot disregard the possibility of leaching occurring along the formed mini cavern and the observed wormhole structure, no additional SEM measurements were carried out. Considering the results of optical microscopy, which revealed minimal permeation aside from the visible wormhole structure, conducting further SEM measurements was deemed unnecessary.

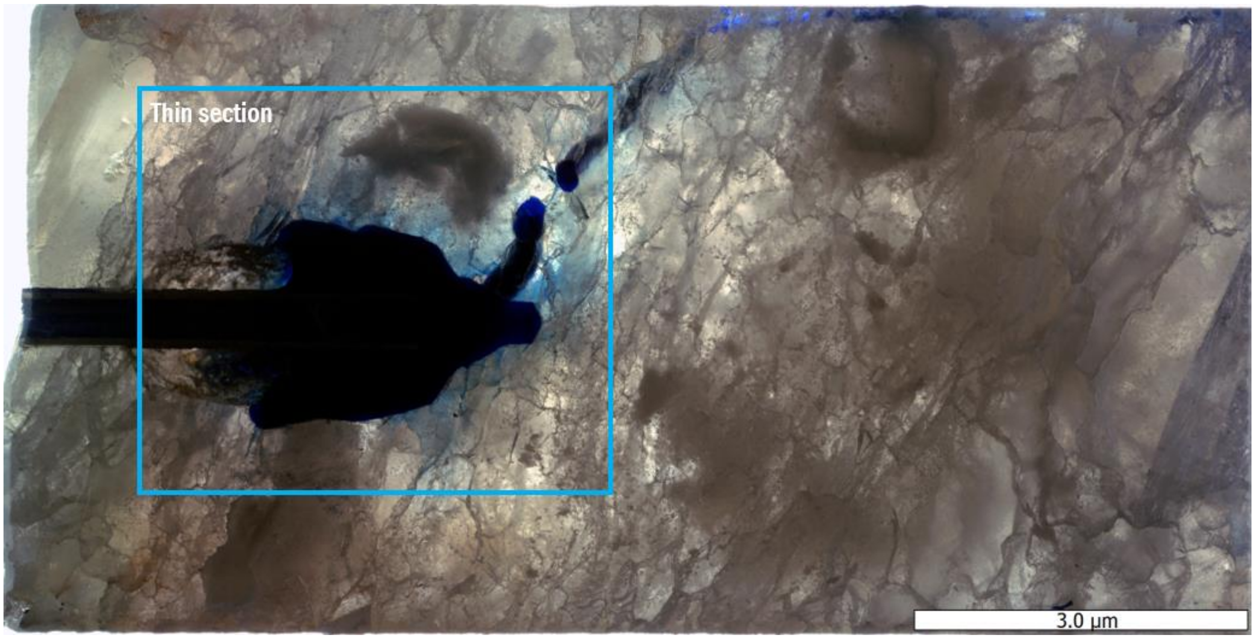

Figure 4: Transmitted light image of the ZW_Perm1 slab indicating the position of the thin section.

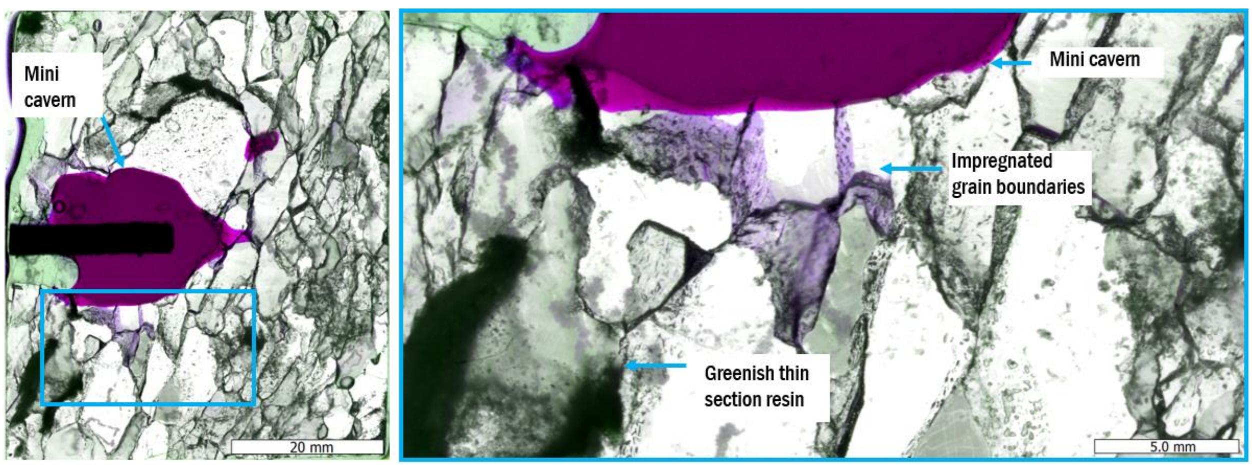

Figure 5: Thin section images PERM1 in transmitted light (left) and detail (right)showing the originally blue coloured epoxy in pink for better visibility.

3.1.3 Permeation experiment

This sample exhibits breakthrough occurring at 42 days, with a brine injection pressure at breakthrough recorded at 10.5 MPa and the maximum pumped brine volume measured at 333 ml (Figure 6). We hypothesize that the wormhole and mini cavern were formed after breakthrough by continued brine injection through the sample, consequently leading to the high value of pumped brine volume. This could potentially have led to leaching and alteration of the surroundings of the tubing (please see IfG report for more details).

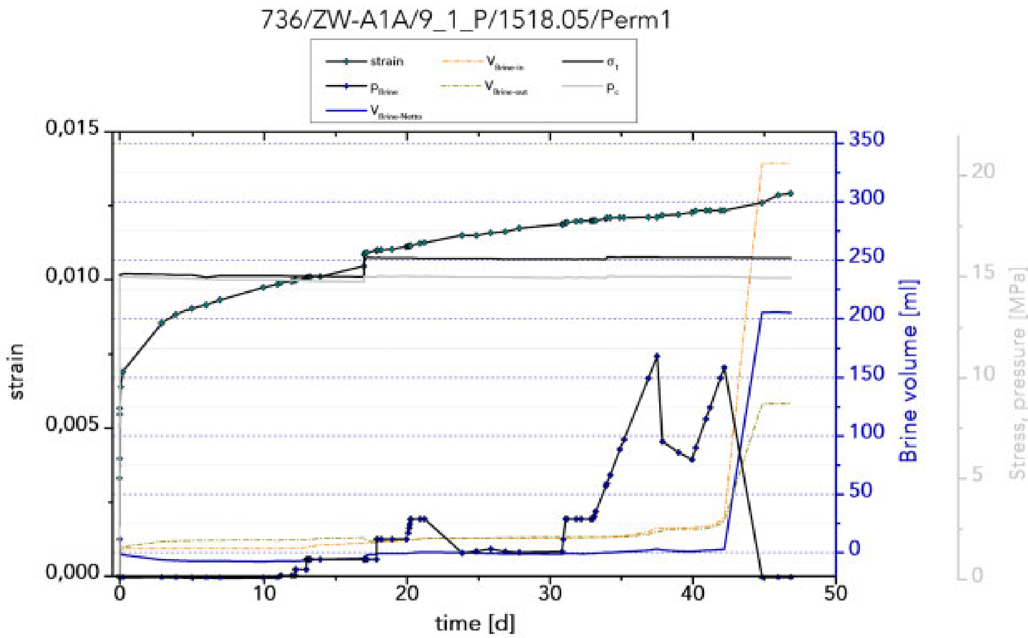

Figure 6: From IfG - Creep curve including pumped brine volume as well as injection pressure recorded during deformation of sample ZW_Perm1.

3.2 ZW_Perm2

ZW_Perm2 was selected from 452,6 meters from well ZWA1A core 2 box number 2 and was classified as almost pure salt with anhydrite dust and halite mega-grains. The selected core piece contains mostly fine-grained polycrystalline matrix halite as well as minor halite mega-grains and a few percent (~1.54 vol%) of anhydrite (Figure 7) in form of a few mm thick bended and ruptured band, located at the other edge of the test cylinder.

Figure 7: Photos of ZW_Perm2 showing the selected core piece before the experiment at ambient light (left), with transmitted light (middle) and after the experiment at ambient light conditions (right) (pictures from IfG).

3.2.1 Micro-CT investigations

The highest fracture density was observed in close proximity to the mini-cavern, gradually decreasing towards the outer edges of the core piece (Figure 8). The shape and orientation of the identified fracture space follow the orientation of the elongated matrix grains, indicating permeation along a dilatant grain boundary network. At the tubing, the cavern bulges, likely due to late-stage leaching processes associated with temporary undersaturation of the brine as a result of high flow rates towards the end of the test. This is also associated with some wormhole-like dissolution pathways that taper-out a few millimetres away from the cavern.

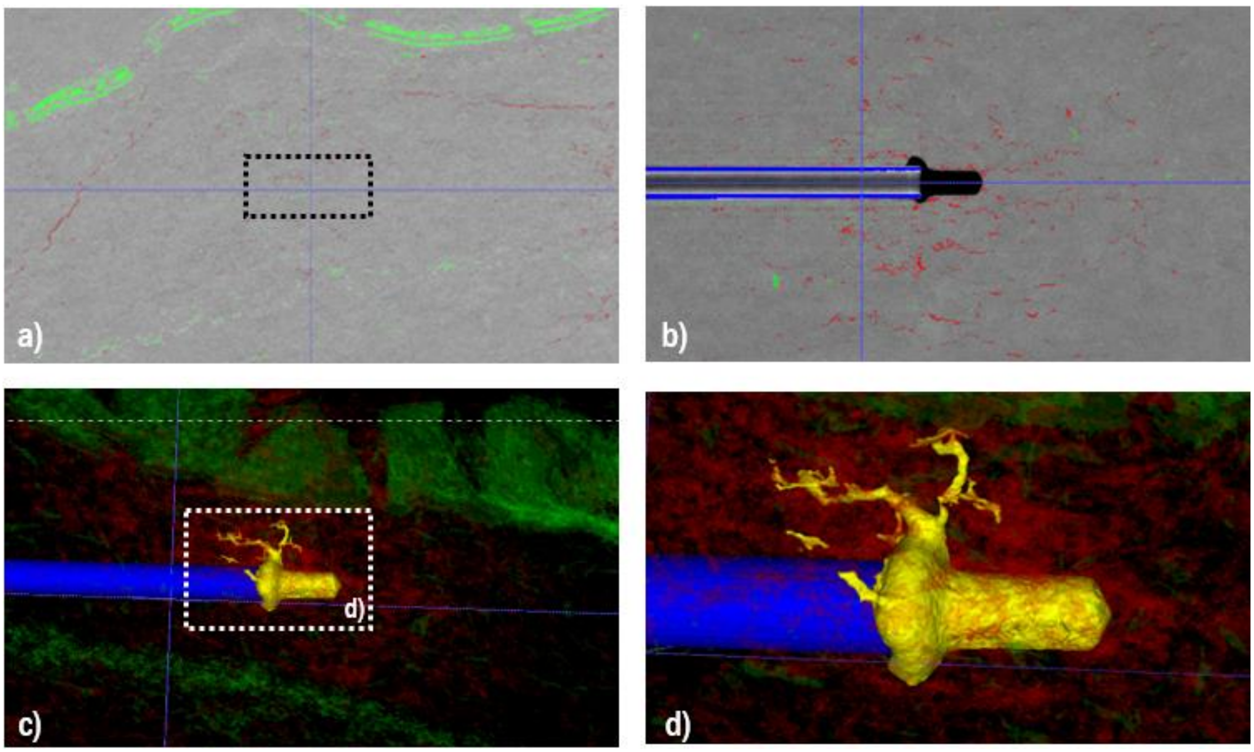

Figure 8: a) ZW_Perm2 cross-section through the Micro-CT scan before permeation, indicating the location of the tubing as well as the phase segmentation with anhydrite in green and fracture space segmented in red. b) cross-section trough micro-CT scan after permeation, showing the phase segmentation. c) 3D visualization of segmented phases including the mini cavern indicated in yellow. d) zoomed-in 3 D visualization highlighting the mini cavern in yellow. For scaling: tube diameter is 0.6 mm.

3.2.2 Microscopy analyses

In the optical microscope we observe an impregnation of blue dyed epoxy along the grain boundaries around the tubing (Figure 9). An anhydrite layer located around 20-30 mm away from the tubing and the mini-cavern does not exhibit clear impregnation by the epoxy (see Figure 10). Please note that for better visibility the hue was changed from blue to pink.

In transmitted light, we observed impregnation of the grain surfaces with blue dyed resin in the vicinity of the mini-cavern (Figure 10 and Figure 11). Nonetheless, this feature does not extend uniformly throughout the core piece to the same degree as observed in the micro-CT images, presumably due to the wetting properties of the resin in relation to the vacuum pressure used for impregnation, which did not allow further penetration of the dilatant grain boundaries in the far field.

When comparing the grain boundaries of a non-treated twin sample with the permeated sample in the optical micrographs (see Figure 11), we noted only minor modifications in the grain boundary structure for boundaries oriented perpendicular to the axial load direction. These boundaries typically dis-played remnants of isolated fluid inclusions. However, grain boundaries parallel to the axial load direction clearly demonstrated dilatancy, as evidenced by resin impregnation and alterations in fluid inclusion imprints, resulting in a more irregular and patchy surface morphology. This observation was confirmed in the SEM (Figure 11d), where we identified dilated grain boundary segments containing resin, alongside closed grain boundary segments occasionally showing efflorescence, indicating the presence of grain boundary fluids prior to thin section preparation (Schenk and Urai, 2004).

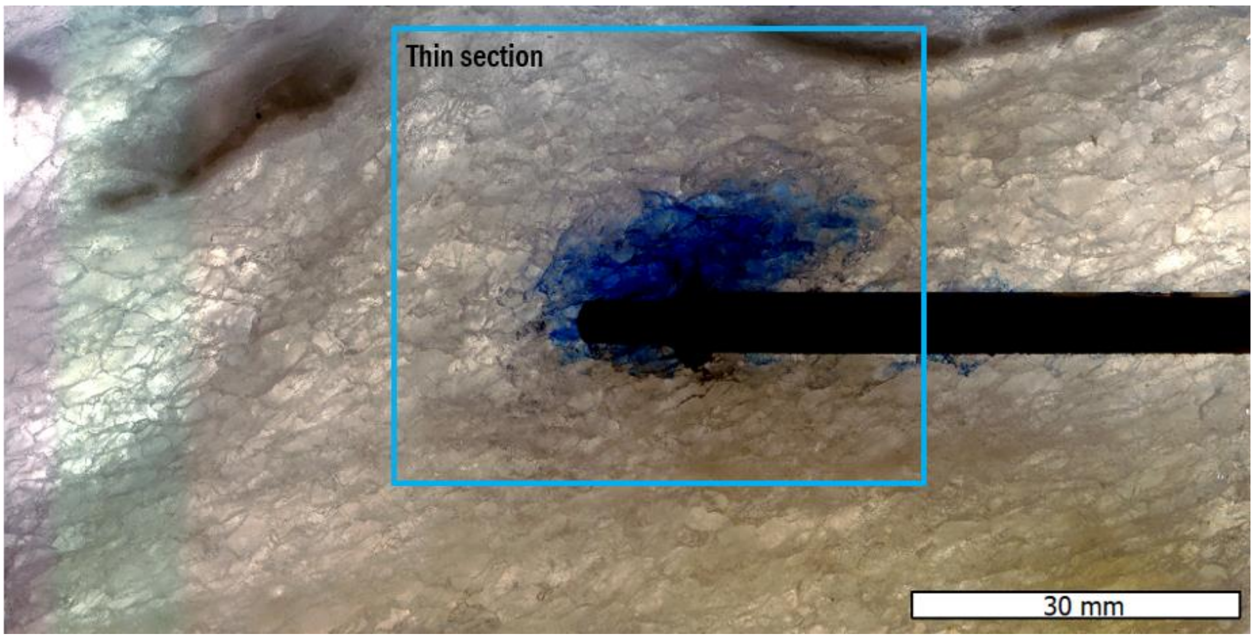

Figure 9: ZW_Perm2 slab in transmitted light.

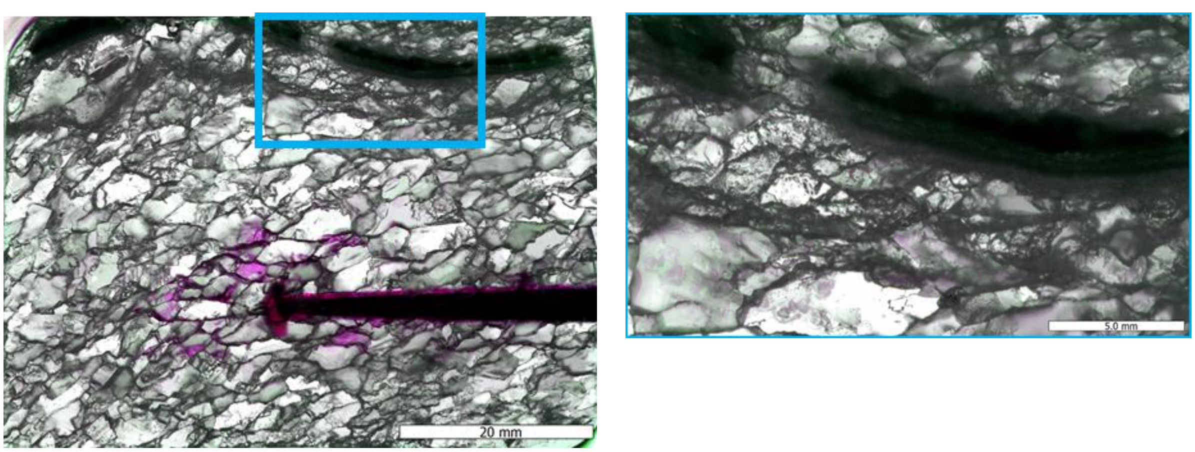

Figure 10: scanned thin section ZW_Perm2 showing the impregnated epoxy in pink (left). Anhydrite layer is not clearly impregnated by the pink epoxy (right).

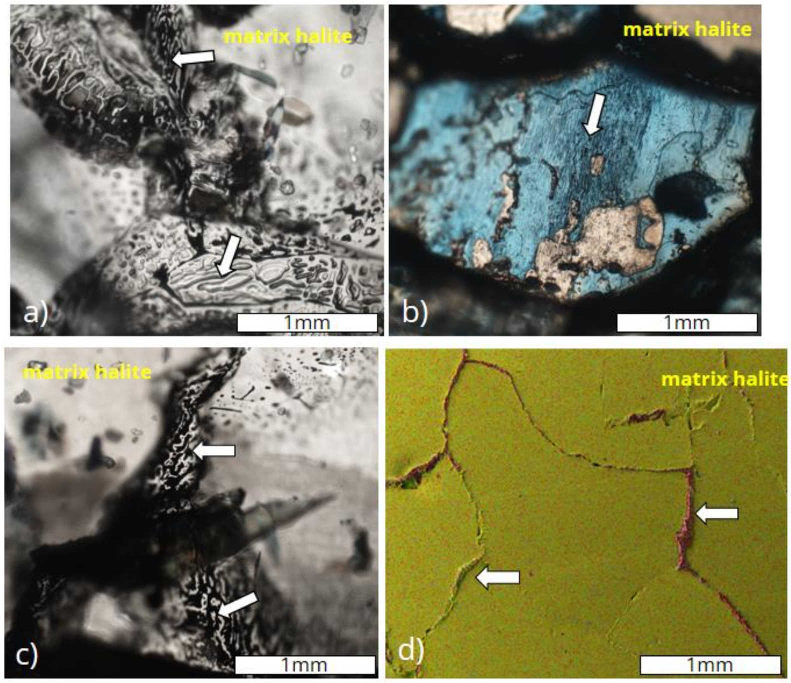

Figure 11: a) thin section micrograph of an untreated twin sample imaged in transmitted light showing grain boundary structure with numerous fluid inclusions, b) thin section micrograph imaged in transmitted light showing dilatant grain boundary, impregnated with resin, oriented parallel to the axial load direction. c) thin section micrograph imaged in transmitted light showing tight grain boundary with fluid inclusions, oriented perpendicular to the axial load direction, d) SEM/EDS micrograph showing resin inside grain boundaries. See the accompanying text for further explanation.

3.2.3 Permeation experiment

The permeation experiment for ZW_Perm2 indicates several breakthroughs. The first breakthrough was observed at p_{brine} of 15.2 MPa after 26 days, a second breakthrough occurred at p_{brine} of 11.7 MPa and a third breakthrough at p_{brine} 15 MPa. Visual inspection by IfG of the deformed sample did not reveal a clear indication of where the breakthrough occurred (Figure 12). Comparing this with the microscopically analyses we presume that a breakthrough would have ultimately occurred due to permeation along grain boundaries.

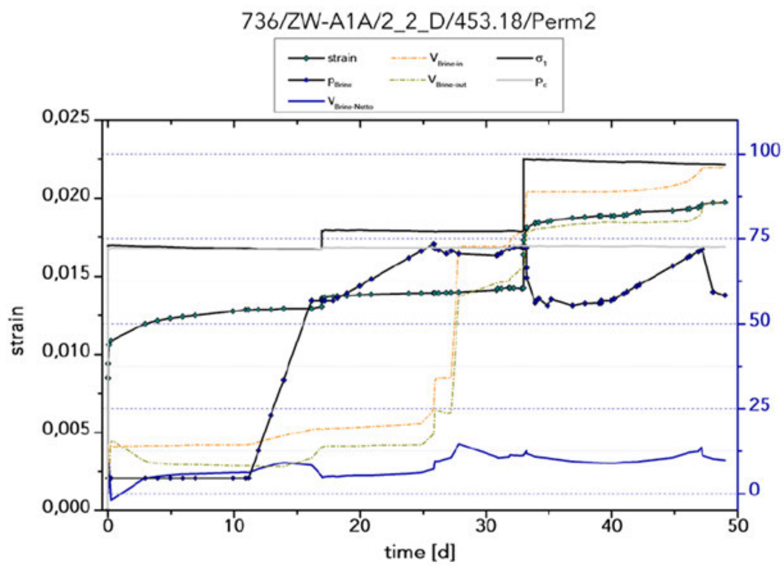

Figure 12: From IfG - Creep curve including pumped brine volume as well as injection pressure recorded during deformation of sample ZW_Perm2.

3.3 ZW_Perm3

The sample primarily comprises polycrystalline halite with thin layers of anhydrite and halite mega-grains. The anhydrite layers are predominantly positioned at the interfaces of halite mega-grains. This sample was chosen due to its high content of halite mega-grains (see Figure 13). The interface between polycrystalline halite and halite mega-grain was selected as the location for placing the tubing and mini-cavern.

Figure 13: Photos of ZW_Perm3 showing the selected core piece before the experiment at ambient light (left), with transmitted light (middle) and after the experiment at ambient light conditions (right) (pictures from IfG).

3.3.1 Micro-CT investigations

Analysis of the Micro-CT data resulted in a fraction of 2.57 vol.% anhydrite and 0.40 vol.% fracture space before permeation (Figure 14). After permeation, no fracture space was detected, and the anhydrite content remained at 2.58 vol.%, indicating consistent results and good comparability of CT-scans as well as the segmentation before and after permeation.

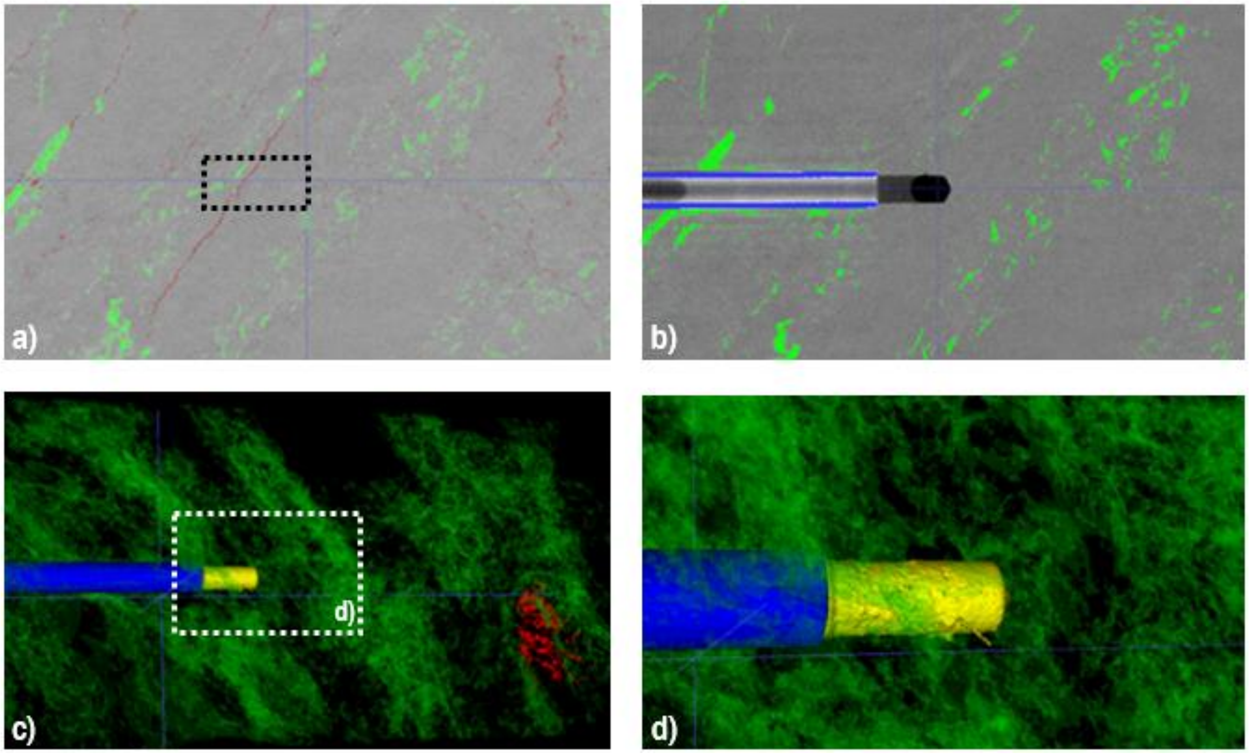

Figure 14: a) ZW_Perm3 cross section though the Micro-CT scan before permeation showing the location of the tubing as well as the phase segmentation with anhydrite in green and fracture space segmented in red. b) ZW_Perm2: Cross section through the Micro-CT scan after permeation showing the phase segmentation. c) 3d visualization of segmented phases and mini cavern in indicated in yellow. d) zoom in 3 d visualization highlighting the mini cavern in yellow. For scaling: tube diameter is 0.6 mm.

3.3.2 Microscopy analyses

ZW_Perm3 was placed in the close vicinity of the interface of the polycrystalline matrix halite with a mega-grain (Figure 15). The mega grain shows micro-fractures oriented perpendicular to the major axis of the mega-grain and with about 30-degree inclination from the vertical core axis.

Optical microscopy using reflected and transmitted light revealed only minor visible intrusion of the blue-dyed resin into the matrix halite grain boundaries (see Figure 15, Figure 16, and **Fehler! Verweisquelle konnte nicht gefunden werden.**). Upon comparing the interface of the matrix grains with the mega-grains near the cavern in the OM, a modification of the grain boundary structure is clearly evident in the form of widespread dilatant zones with only a few remaining grain-to-grain contacts (**Fehler! Verweisquelle konnte nicht gefunden werden.**).

SEM investigation showed the majority of impregnated grain boundaries in the polycrystalline halite above the mega-grain. However, high-resolution SEM on the etched thin section surface clearly depicted resin impregnation at the interface of the mega-grain with the polycrystalline halite matrix grains (see Figure 15). Additionally, some impregnations were also detected below the mega-grains, indicating permeability of the mega-grain to the dyed resin.

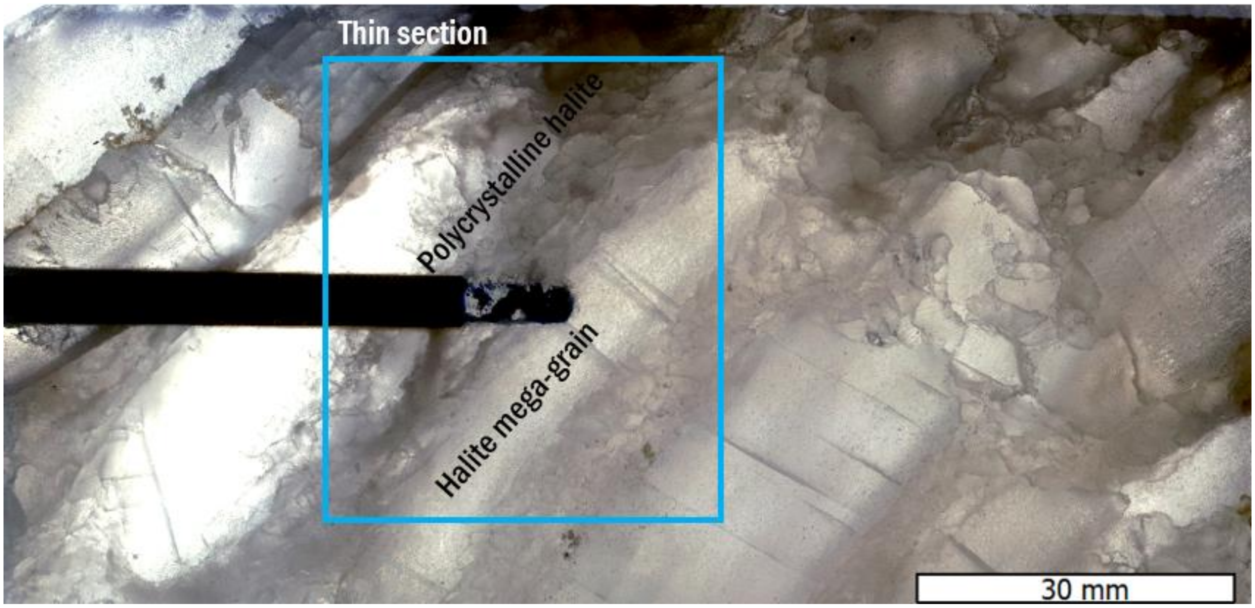

Figure 15: Transmitted light image of the ZW_Perm3 slab indicating the position of the thin section.

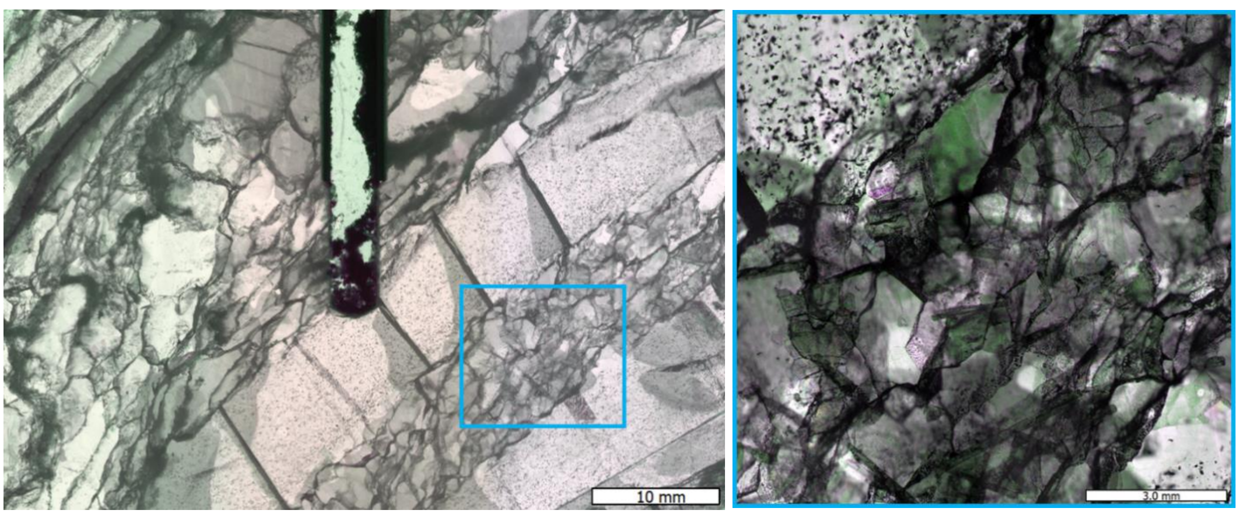

Figure 16: Thin section in transmitted light of sample ZW_Perm3 (left) and reflected light microscopy of area of interest (right) indicating impregnated epoxy in pink. In green is the underlying resin of the thin section preparation.

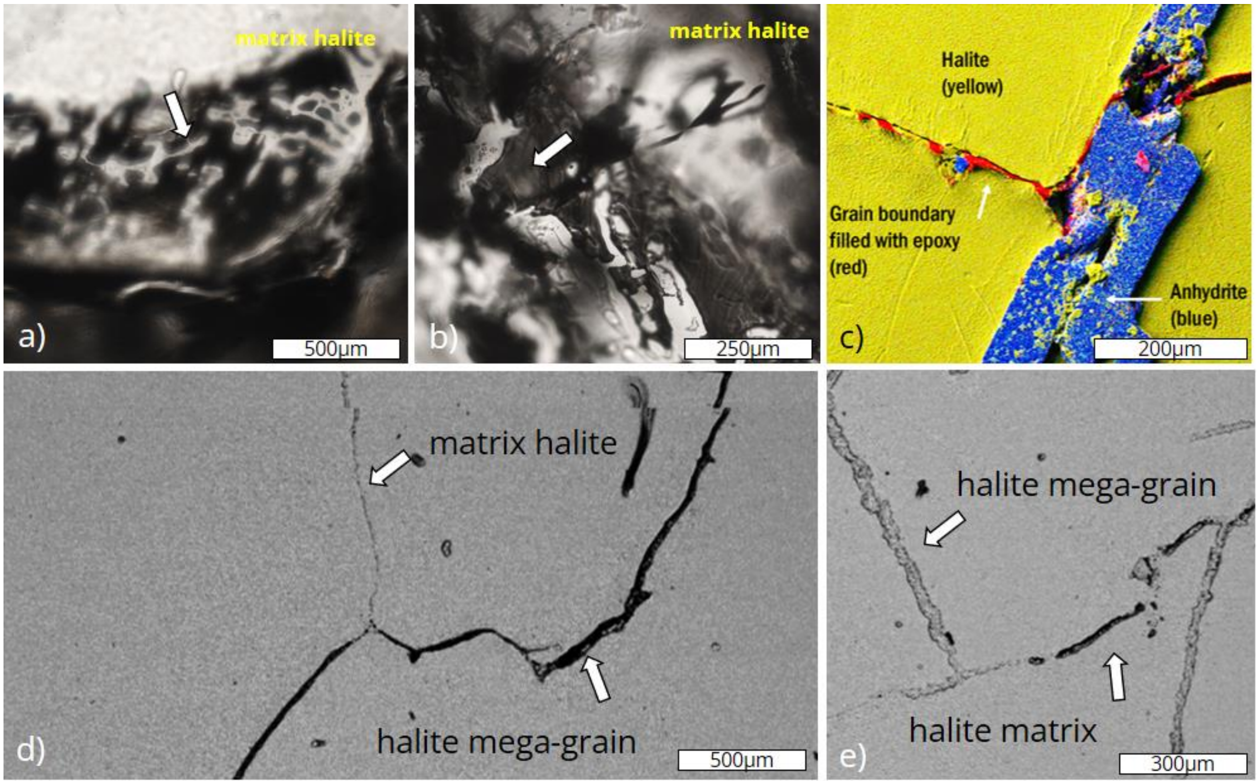

Figure 17 a) thin section micrograph of an untreated twin sample imaged in transmitted light showing interface of matrix halite with a mega-grain, b) thin section micrograph of sample Perm3 imaged in transmitted light showing dilatant interface if matrix halite with a mega-grain, c) SEM/EDS micrograph showing, resin (C, red colour) inside grain boundary oriented parallel to σ1 cross-cutting an anhydrite grain, d) matrix halite/mega-grain interface cross-section imaged in the SEM filled with resin (black diagonal line), matrix halite grain boundary (upper arrow) shows efflorescence, f) matrix halite/mega-grain interface cross-section imaged in the SEM filled with resin (lower arrow), matrix halite grain boundary (upper arrow) shows efflorescence.

3.3.3 Permeation experiment

ZW_Perm3 indicated no breakthrough after four days at isostatic conditions, only after increasing the pressure to p_{brine} to 16.4 MPa a breakthrough was observed. After a resting phase of 14 days the pressure was increased to p_{brine} of 2 MPa without any further breakthrough indicating some healing processes within the sample (Figure 18) (for more detail please see IfG report). The microscopy analyses yield no results that would explain the healing capacity of this sample. The only suggestion is that the healing might happened in the polycrystalline halite matrix, but this could not be proven with microscopy images.

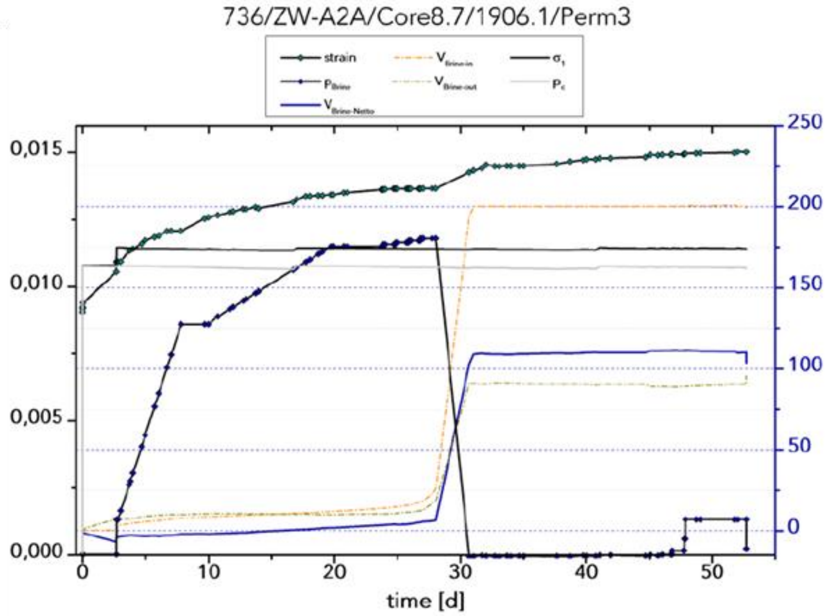

Figure 18: From IfG - Creep curve including pumped brine volume as well as injection pressure recorded during deformation of sample ZW_Perm3.

3.4 ZW_Perm4

This sample was selected from a depth of 592.1 m from well ZW-A3A core number 1 and box number 2. In the selected core piece, the anhydrite is primarily concentrated in nodules, with only minimal anhydrite dust visible. The core piece exhibits a mylonitic fabric and is predominantly composed of a fine- to coarse-grained matrix halite (Figure 19). Furthermore, an a few mm thick anhydrite band is located at the other edge of the test cylinder. The tubing and mini cavern were placed into matrix halite in a location with accumulated anhydrite nodules.

Figure 19: Photos of ZW_Perm4 showing the selected core piece before the experiment at ambient light (left), with transmitted light (middle) and after the experiment at ambient light conditions (right) (pictures from IfG).

3.4.1 Micro-CT investigations

In sample ZW_Perm4 the segmented anhydrite fraction is relatively low, at 6.02 vol.% and the segmented fracture space is 0.13 vol.% before the permeation experiment (Figure 20). After the permeation 4.57 vol.% of anhydrite and 0.0 vol.% of fracture space were segmented. No fractures are detected at a resolution of 74 µm.

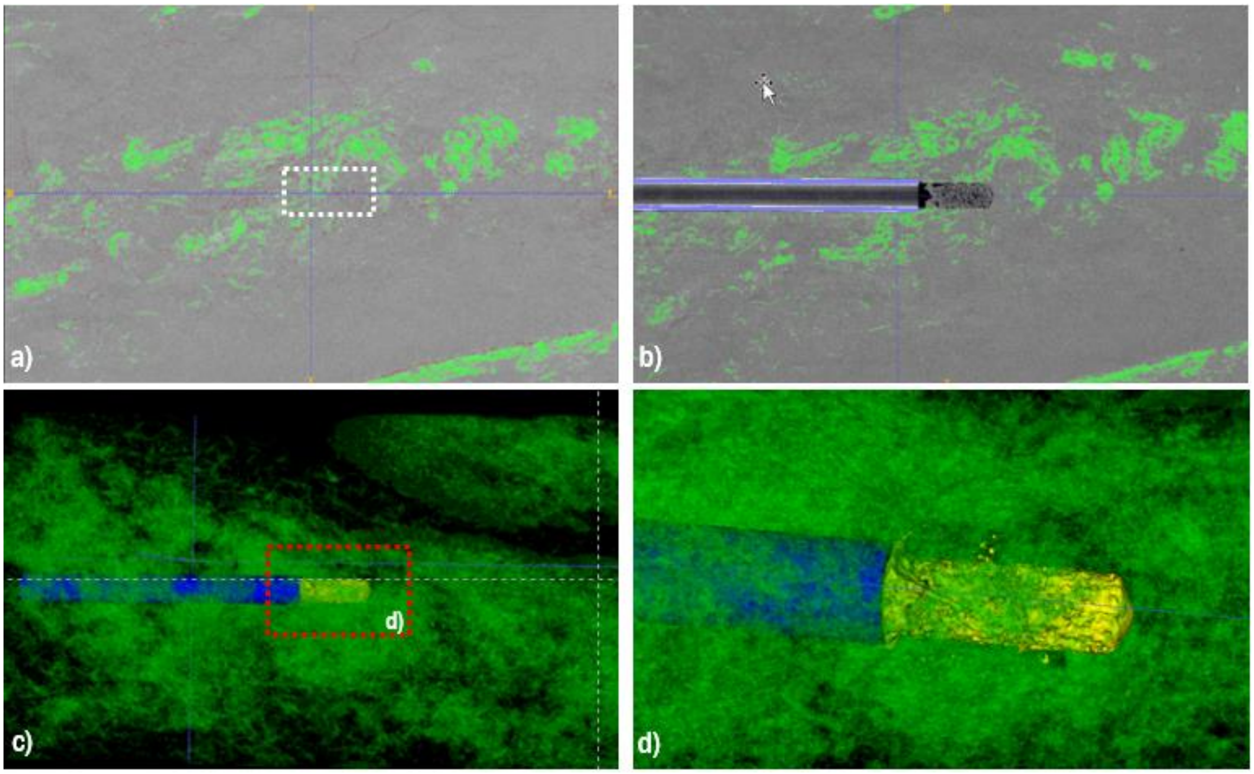

Figure 20: a) ZW_Perm4 cross section though the Micro-CT scan before permeation showing the location of the tubing as well as the phase segmentation with anhydrite in green and fracture space segmented in red. b) ZW_Perm2: Cross section through the Micro-CT scan after permeation showing the phase segmentation. c) 3d visualization of segmented phases and mini cavern in indicated in yellow. d) zoom in 3 d visualization highlighting the mini cavern in yellow. For scaling: tube diameter is 0.6 mm.

3.4.2 Microscopy analyses

In sample ZW_Perm4 the mini-cavern was placed in a coarse-grained polycrystalline halite matrix alternating with anhydrite dust layers (Figure 21). Blue-dyed epoxy was visible in the vicinity of the mini-cavern and along the tubing. The thin section shows some impregnation of epoxy along grain boundaries but not as abundant as the slab images suggested (Figure 22). A BIB SEM cross-section targeting an anhydrite layer close to the tubing shows dilatant grain boundaries and open micro pore-space, which was not filled with epoxy (Figure 23). The anhydrite layer was therefore not impregnated, indicating the anhydrite at this location is compact/dense. Grain boundaries in comparison to the un-permeated twin sample appear also unchanged and indicate no permeation. (**Fehler! Verweisquelle konnte nicht gefunden werden.**).

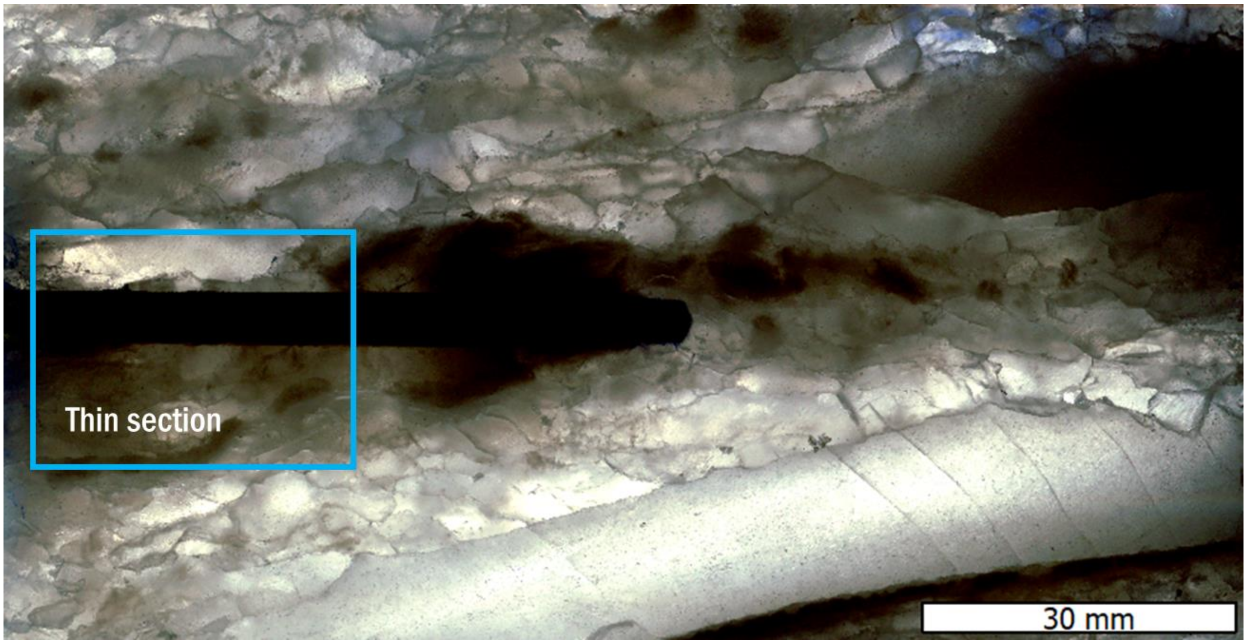

Figure 21: Transmitted light image of the ZW_Perm4 slab indicating the position of the thin section.

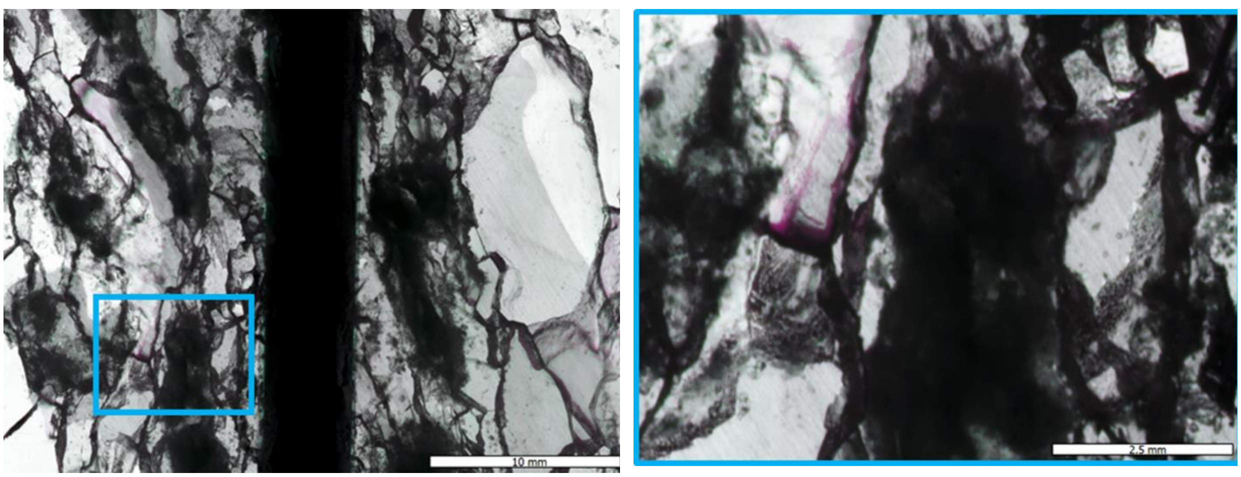

Figure 22: Transmitted light image of the thin section of ZW_Perm4, highlighting impregnated areas coloured in pink. The image on the right displays regions with impregnated epoxy, depicted in pink, along grain boundaries.

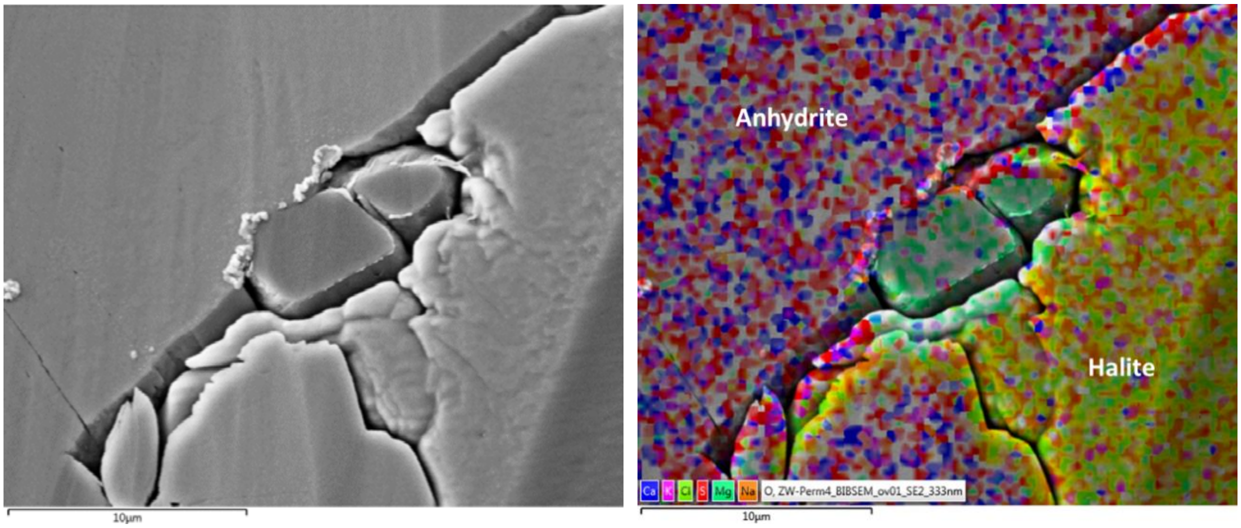

Figure 23: BIBSEM images from ZW_Perm4 indicating open grain boundaries along anhydrite-halite interface.

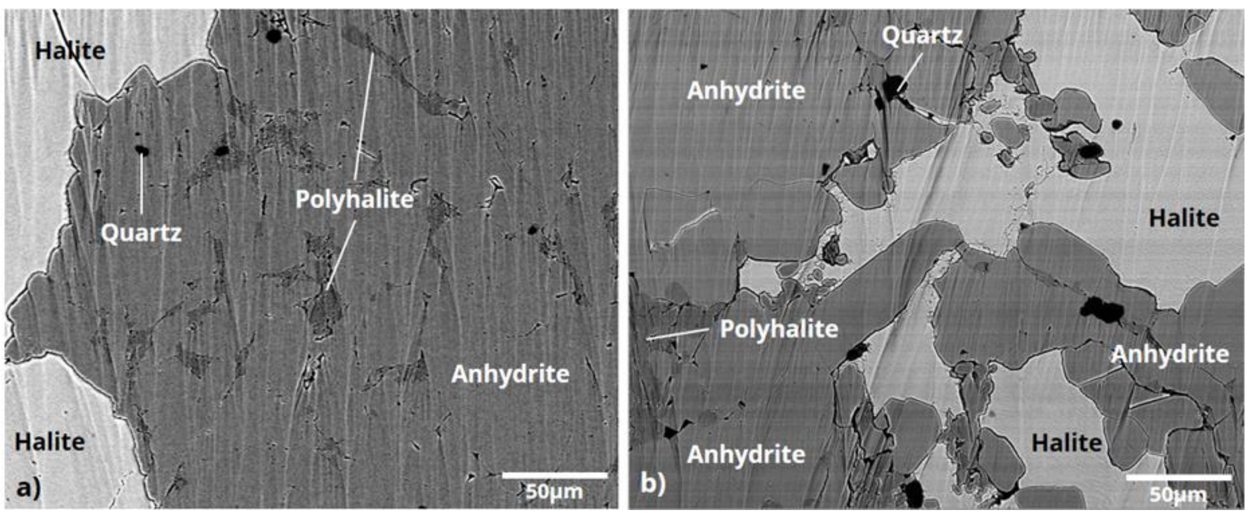

Figure 24: BIB-SEM micrographs showing a) twin sample with anhydrite containing polyhalite in contact with matrix halite and b) anhydrite in Perm4 showing no alteration of the initial structures or impregnation of the grain boundaries/pores with resin.

3.4.3 Permeation experiment

The permeation experiment for sample ZW_Perm4 exhibited a distinctive behaviour, as the incremental increase in injection pressure did not result in an identifiable breakthrough. Despite maintaining a constant injection pressure, the flow rate increased, yet no breakthrough was observed (Figure 25). This could account for the slight impregnation observed in the optical and scanning microscopy of sample ZW-Perm4, or perhaps the anhydrite layers facilitate some level of permeation. However, this has yet to be conclusively demonstrated or disproven.

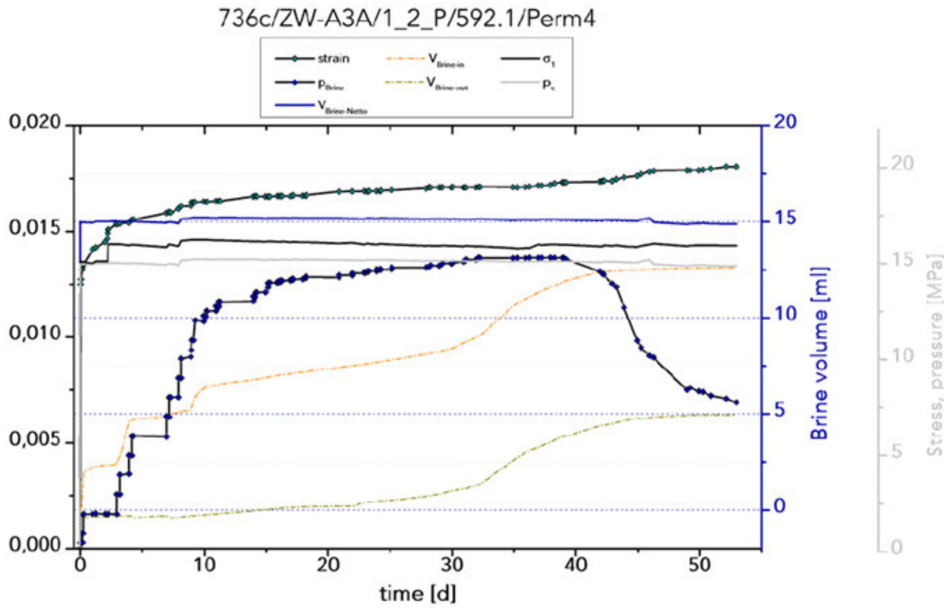

Figure 25: From IfG - Creep curve including pumped brine volume as well as injection pressure recorded during deformation of sample ZW_Perm4.

3.5 ZW_Perm5

ZW-Perm5 was chosen from a depth of 991.1 m in well ZW-A3A core number 2 and box slab number 1. It comprises a predominantly coarse-grained matrix halite with scattered layers of anhydrite dust or small nodules. Exhibiting a mylonitic fabric, the selected core piece reveals minor halite mega-grains (Figure 26). The tubing was positioned between matrix halite and anhydrite dust.

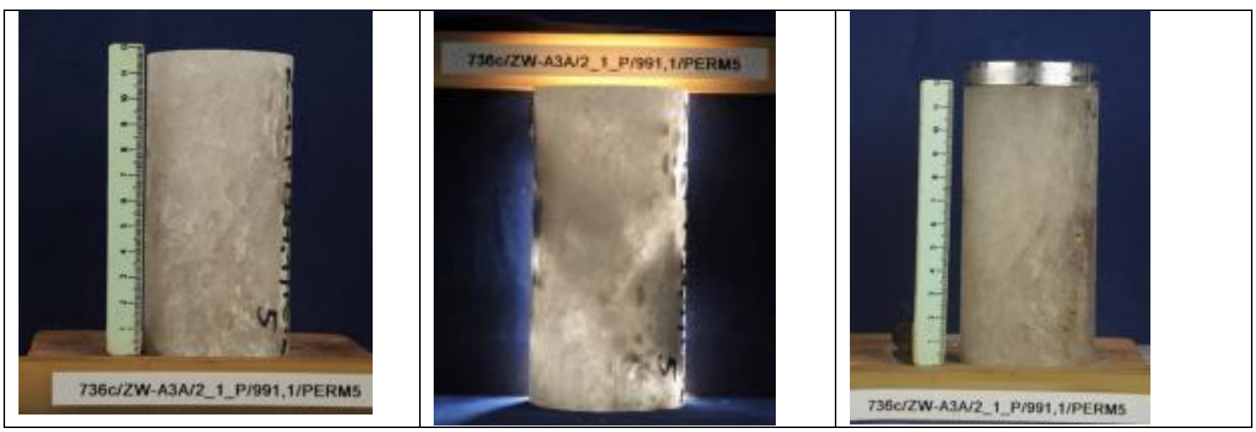

Figure 26: Photos of ZW_Perm5 showing the selected core piece before the experiment at ambient light (left), with transmitted light (middle) and after the experiment at ambient light conditions (right) (pictures from IfG).

3.5.1 Micro-CT investigation

Before the experiment, this sample exhibited the most substantial presence of anhydrite in the phase segmentation in comparison with the other samples, quantified at 12.9 vol.%, accompanied by minimal fracture space at 0.39 vol.% (Figure 27). Following permeation, the anhydrite content decreased to 10.9%, with no fracture space segmented at a resolution of 74 µm. Notably, during the experiment, a leached mini-cavern emerged, likely stemming from the experiment setup persisting in pumping after breakthrough, consequently leaching the area surrounding the tubing which was later filled by the dyed epoxy. This phenomenon is highlighted in yellow.

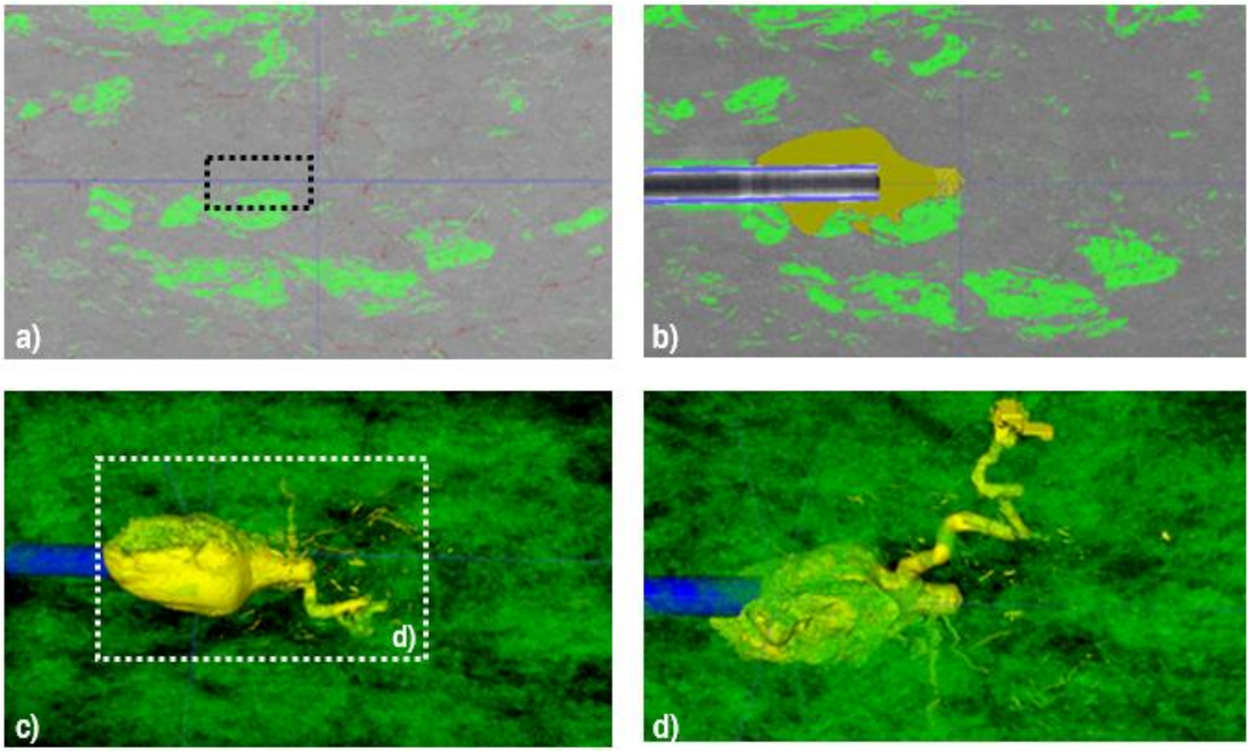

Figure 27: a) ZW_Perm5 cross section though the Micro-CT scan before permeation showing the location of the tubing as well as the phase segmentation with anhydrite in green and fracture space segmented in red. b) ZW_Perm2: Cross section through the Micro-CT scan after permeation showing the phase segmentation. c) 3d visualization of segmented phases and mini cavern in indicated in yellow. d) zoom in 3 d visualization highlighting the mini cavern in yellow. For scaling: tube diameter is 0.6 mm.

3.5.2 Microscopy analyses

Both optical and electron microscopy show evidence of blue-dyed epoxy permeating along grain boundaries and encircling the anhydrite layer situated on the right-hand side of the tubing (Figure 28 and Figure 29). Scanning microscopy, however, does not distinctly show impregnation of the anhydrite by the epoxy (Figure 30). Instead, it reveals dyed epoxy present in isolated spots within the anhydrite. At present, it remains unclear whether the anhydrite has been an effective permeation pathway or if the occurrence of the dyed resin within the porous anhydrite was possible after the permeation test as a high fluid-flow rate after the breakthrough allowed the mobilization of clay fines and or polyhalite from the anhydrite pores creating well connected pore-space within the previously low-permeable anhydrite inclusions (Schmatz et al., in press, KEM-28 study).

Additionally, we compared typical grain boundaries from a twin sample with an open grain boundary from the permeated sample to get insights into the grain boundary surface structure and the underlying processes (Figure 31). The grain boundary surface of the twin sample exhibits fluid inclusion arrays of variable size and shape. Similarly, the open grain boundary in the permeated sample, oriented parallel to the vertical core axis, displays a comparable surface structure with fluid imprints covered by the blue dyed epoxy. We hypothesize that in this scenario, we observe grain boundaries that undergoes slight dilation during permeation due to the change in pore pressure, yet the gran surface largely remains unchanged throughout the process.

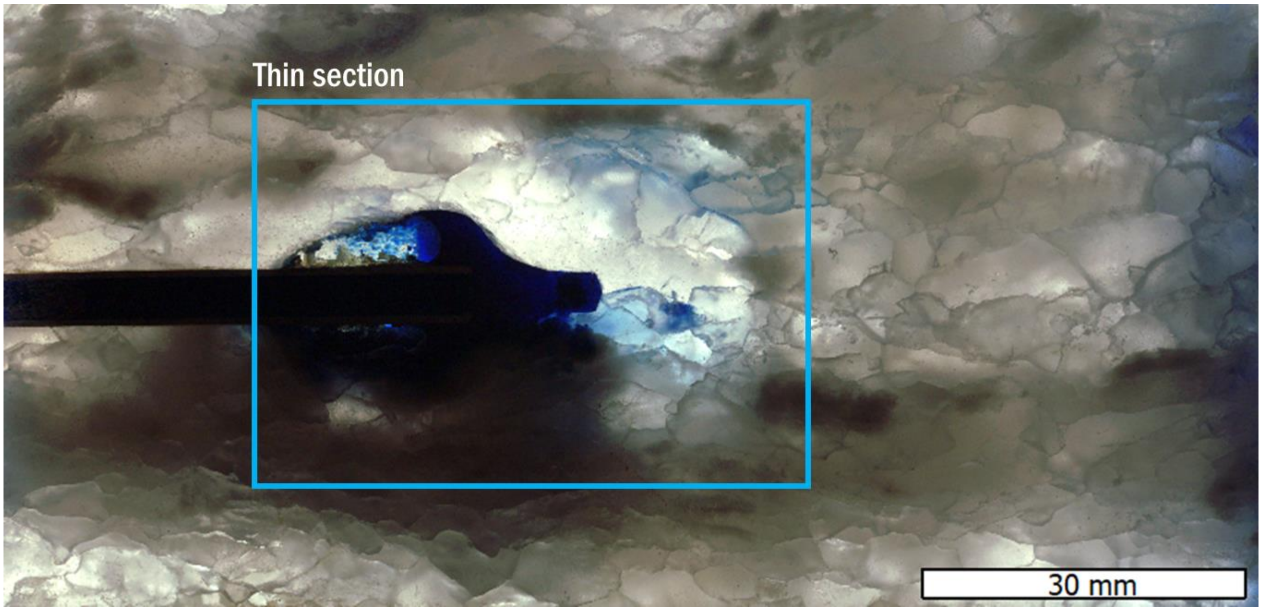

Figure 28: Transmitted light image of the ZW_Perm5 slab indicating the position of the thin section.

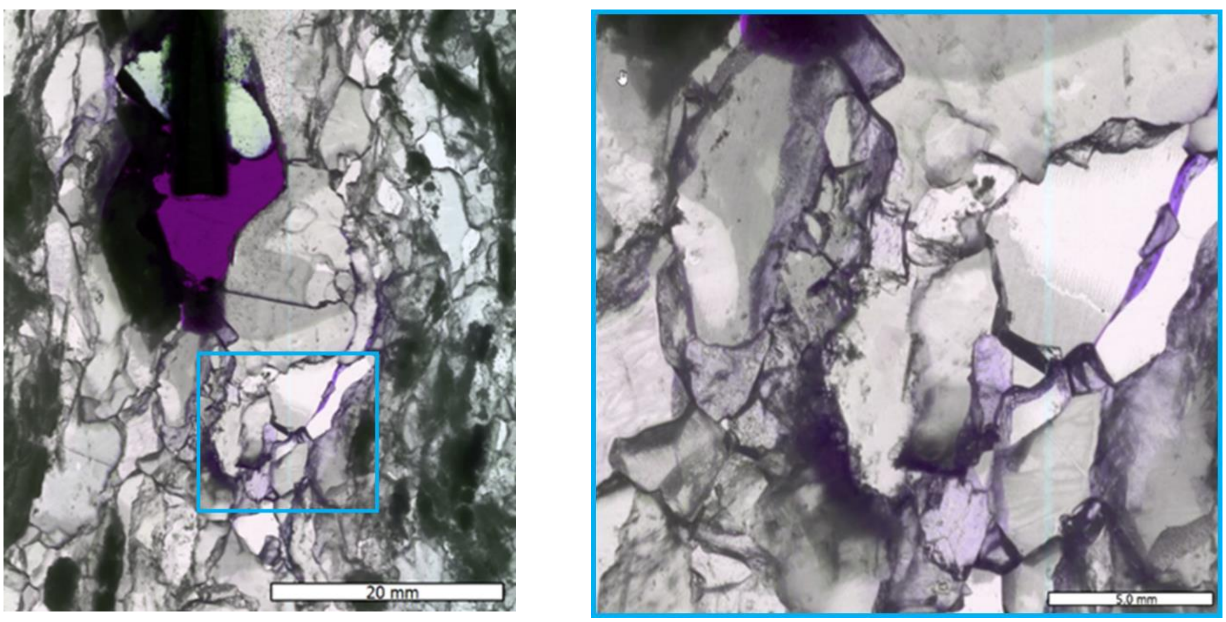

Figure 29: Transmitted light image of the thin section of ZW_Perm5, highlighting impregnated areas coloured in pink. The image on the right displays regions with impregnated epoxy, depicted in pink, along grain boundaries.

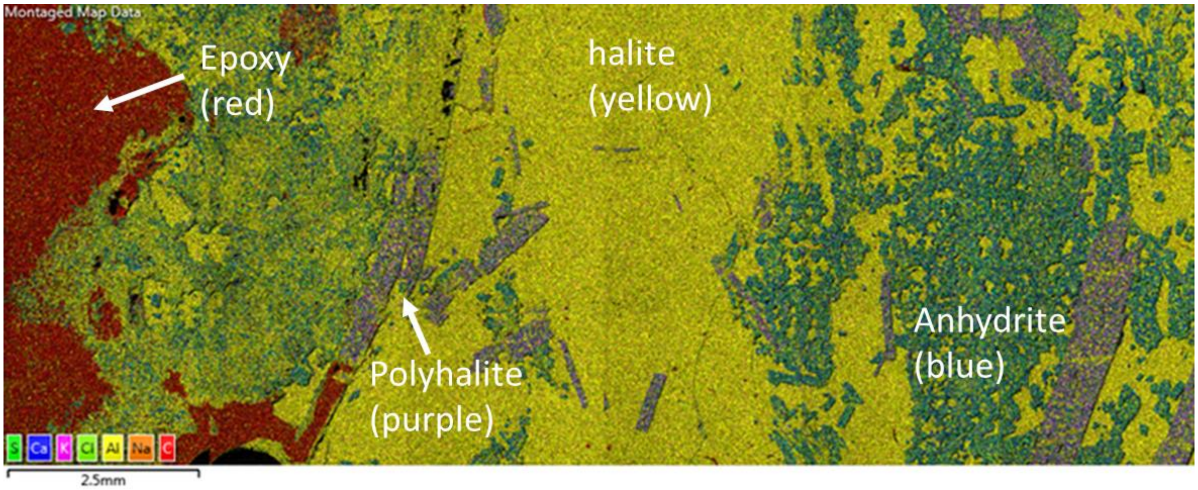

Figure 30: SEM images for ZW_Perm5 illustrating the dyed epoxy next to the anhydrite.

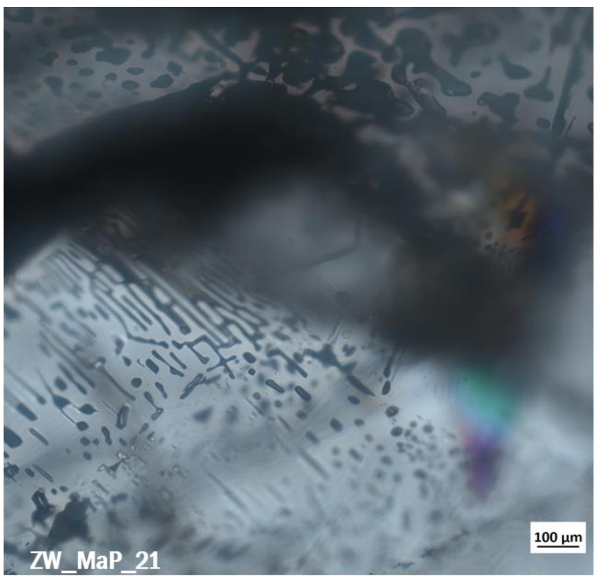

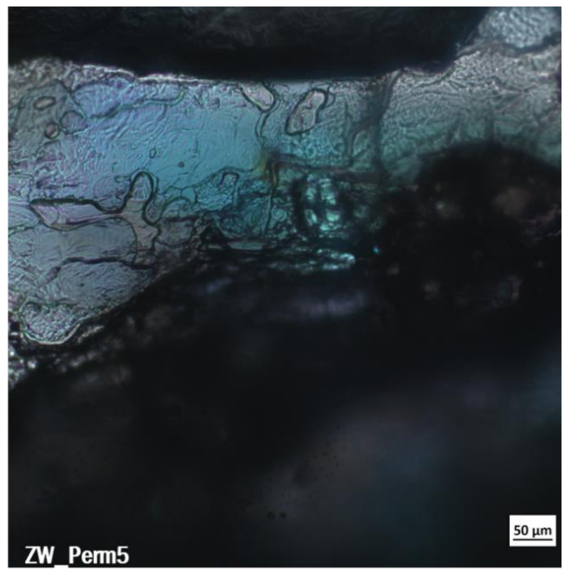

Figure 31: Comparison of the grain boundary surface on the left side of twin sample ZW_MaP_21 with the grain boundary surface from sample ZW_Perm5.

3.5.3 Permeation experiment

For this sample, the injection pressure reached 12.0 MPa, with only a slight increase in flow rate. Subsequently, the pressure was further raised to 12.8 MPa, leading to an increase in flow rate. Following a 6-day pause and a pressure drop, the injection pressure was raised again to 13.6 MPa, although no breakthrough was observed, it may have occurred eventually (Figure 32). Here it’s not clear, when the observed leaching around the tubing took place.

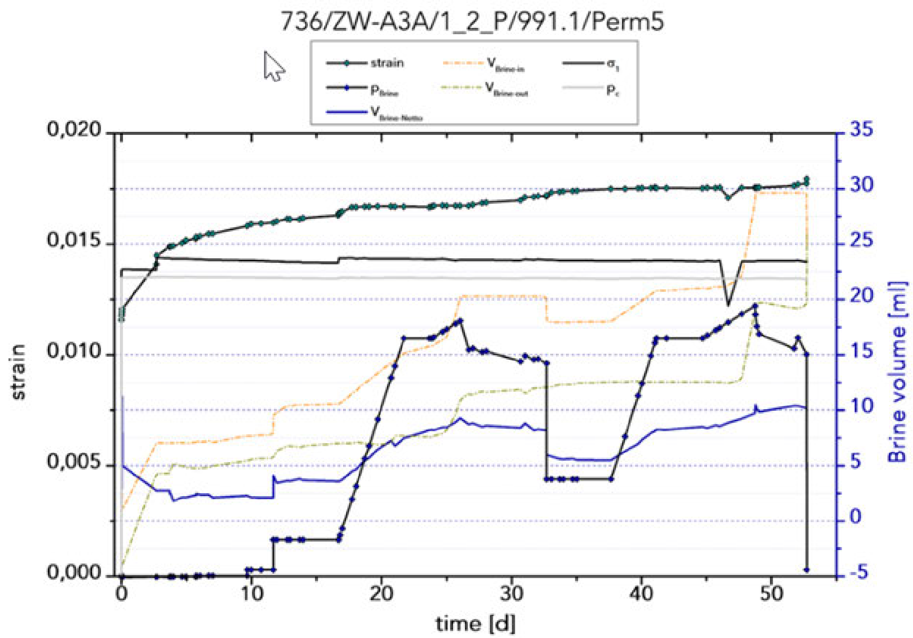

Figure 32: From IfG - Creep curve including pumped brine volume as well as injection pressure recorded during deformation of sample ZW_Perm5.

3.6 ZW_Perm6

This sample was selected from well ZW_A3A core number 6 and box slab number 5 from a depth of 1444.5m. The selected core piece was chosen due to its mylonitic fabric and a relatively high variable halite matrix in terms of grain size and shape. Anhydrite is visible as nodules and also as minor anhydrite dust (Figure 33). Halite mega-grains are located in the middle part of the selected core piece. The tubing was positioned within the coarse-grained matrix halite, with anhydrite layers situated at a slight distance.

Figure 33: Photos of ZW_Perm6 showing the selected core piece before the experiment at ambient light (left), with transmitted light (middle) and after the experiment at ambient light conditions (right) (pictures from IfG).

3.6.1 Micro-CT investigations

The Micro-CT data shows a segmented anhydrite content of 6.05 vol.% and a segmented fracture space of 0.49 vol.% before permeation (Figure 34). Thereafter the segmented anhydrite content is decreased to 4.90 vol. % and no fracture space is segmented at a resolution of 41 µm.

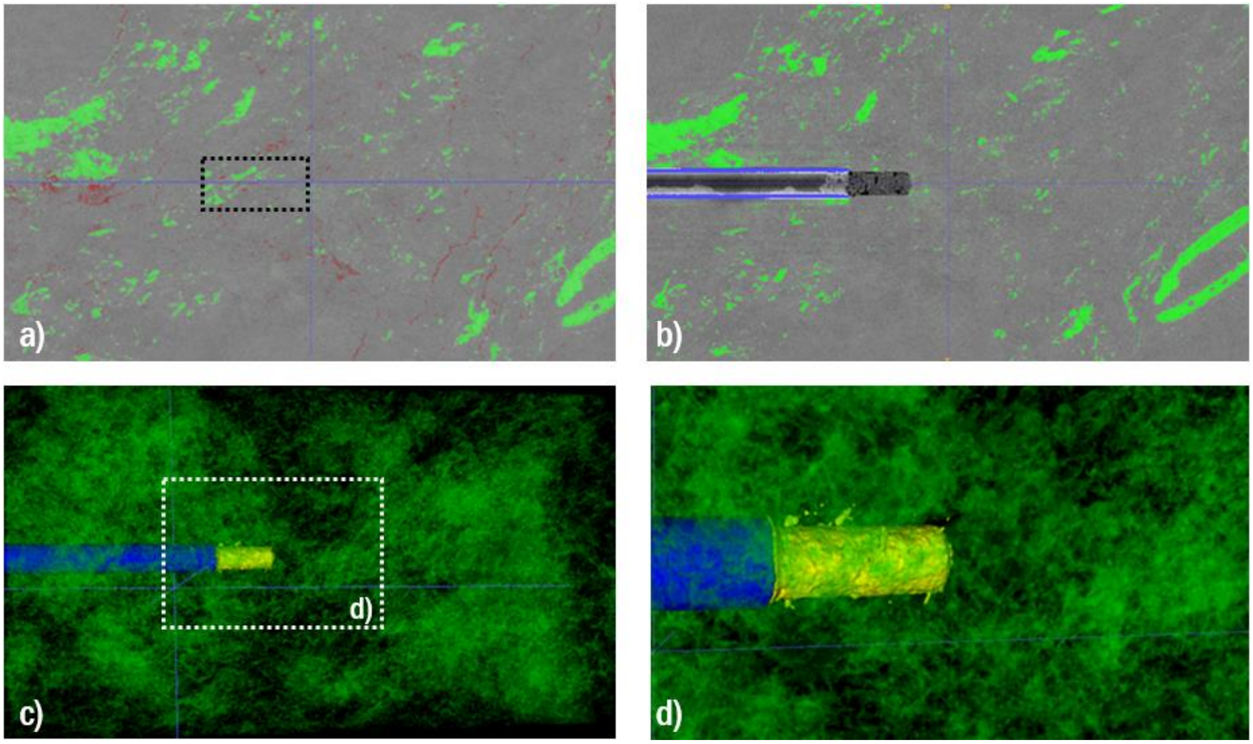

Figure 34 a) ZW_Perm6 cross section though the Micro-CT scan before permeation, indicating the location of the tubing as well as the phase segmentation with anhydrite in green and fracture space in red. b) cross-section thorough Micro-CT scan after permeation, showing the phase segmentation. c) 3D visualization of segmented phases including mini caverns indicated in yellow. d) zoomed-in 3 D visualization highlighting the mini cavern. For scaling: tube diameter is 0.6 mm.

3.6.2 Microscopy analyses

The optical and scanning electron microscopy results reveal the dyed epoxy impregnating along grain boundaries. However, only minor impregnation was visible in the scanned thin section (Figure 35 and Figure 36). With the scanning electron microscopy an impregnation along grain boundaries was observed and is illustrated in Figure 37, including fluid imprints along grain boundaries. The grain boundary surface of the twin sample exhibits fluid imprints. Similarly, the open grain boundary in the permeated sample, oriented parallel to sigma 1, displays a comparable surface structure with fluid imprints. We hypothesize that in this scenario, we observe a dilatant grain boundary that undergoes slight opening during permeation due to applied pressure, yet largely remains unchanged throughout the process (

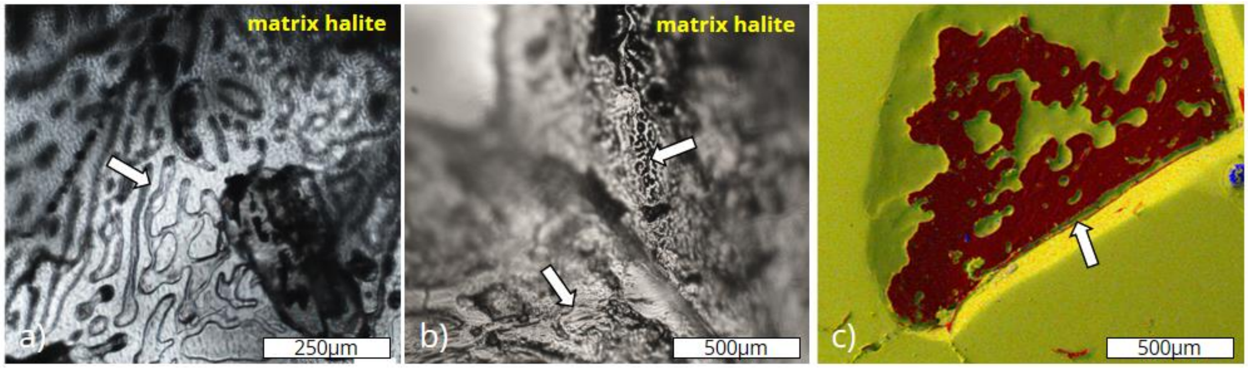

Figure 38 a) thin section micrograph of an untreated twin sample imaged in transmitted light showing grain boundary structure with numerous fluid inclusions, b) thin section micrograph imaged in transmitted light showing tight grain boundary with fluid inclusions, oriented perpendicular to the axial load direction, c) SEM/EDS micrograph showing, resin (C, red colour) covered grain surface oriented parallel to the axial load direction.

).

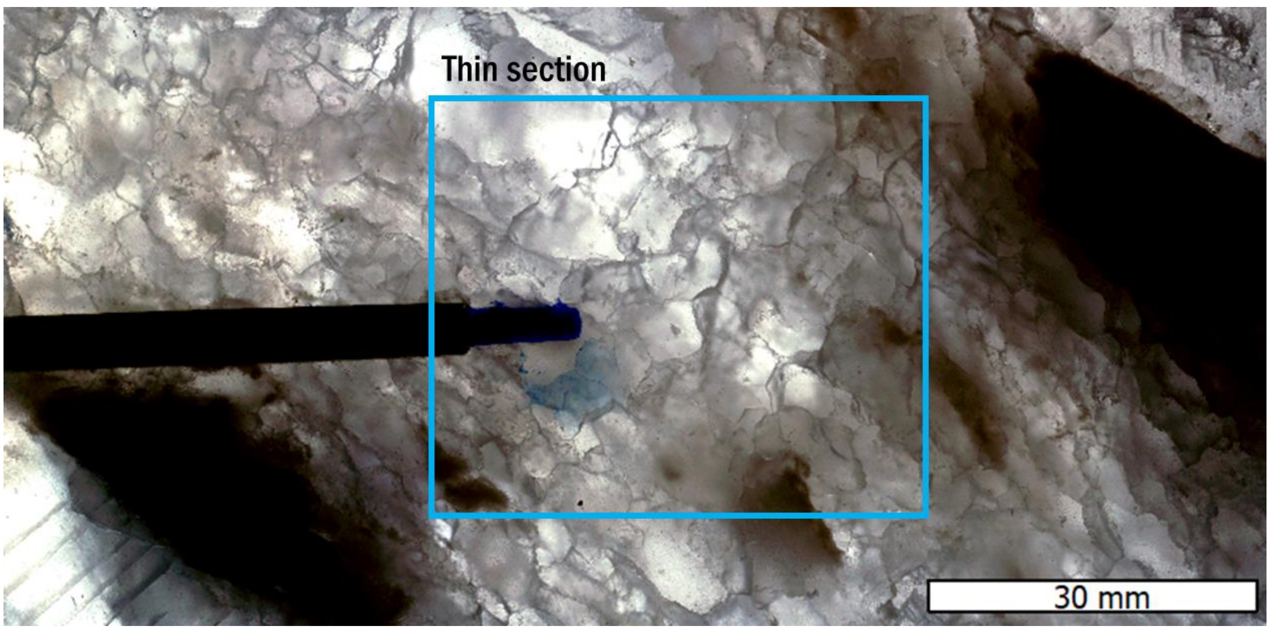

Figure 35: Transmitted light image of the ZW_Perm6 slab indicating the position of the thin section.

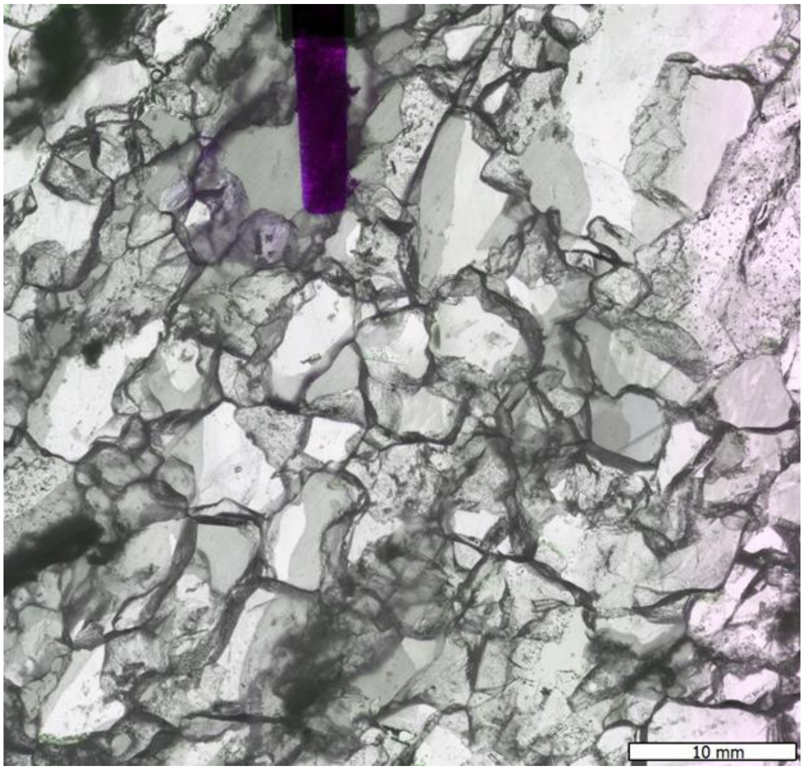

Figure 36: Thin section of ZW_Perm6 in transmitted light.

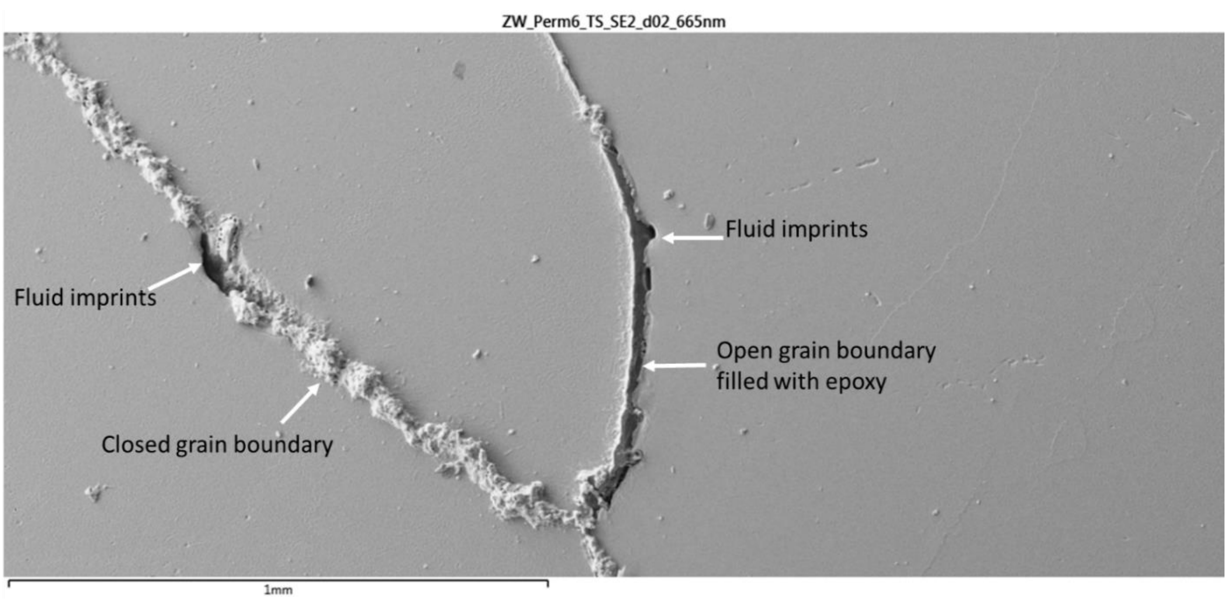

Figure 37: Grain boundaries for ZW_Perm6 observed using the SEM.

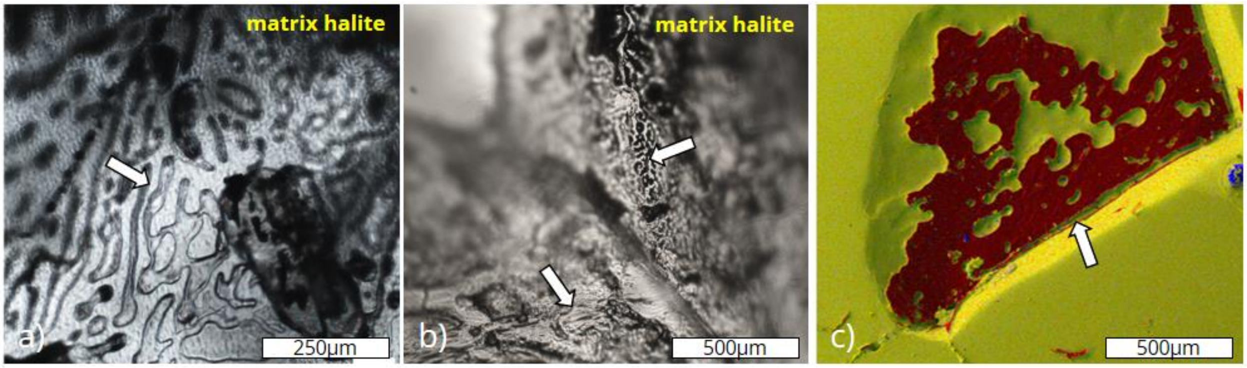

Figure 38 a) thin section micrograph of an untreated twin sample imaged in transmitted light showing grain boundary structure with numerous fluid inclusions, b) thin section micrograph imaged in transmitted light showing tight grain boundary with fluid inclusions, oriented perpendicular to the axial load direction, c) SEM/EDS micrograph showing, resin (C, red colour) covered grain surface oriented parallel to the axial load direction.

3.6.3 Permeation experiment

The permeation experiment with ZW_Perm6 demonstrated no breakthrough despite incrementally increasing injection pressure up to p_{brine} 15.5 MPa. Only slight variations in flow rate were observed throughout this phase (Figure 39). We hypothesize that the coarser-grained halite matrix is permeating along grain boundaries and potentially requiring more time to do so, and a breakthrough may have ultimately occurred.

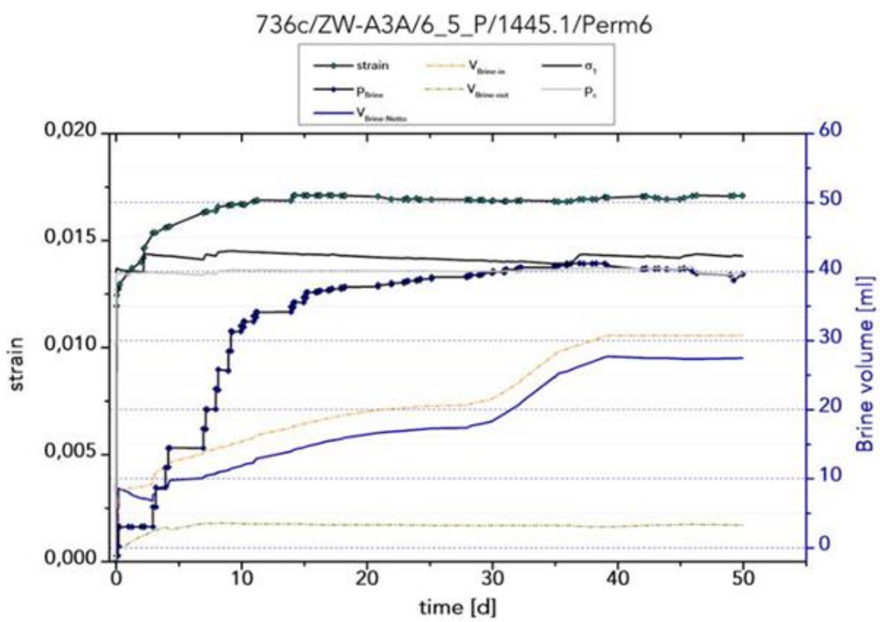

Figure 39: From IfG - Creep curve including pumped brine volume as well as injection pressure recorded during deformation of sample ZW_Perm6.

4 Conclusions and recommendations

Permeation tests conducted on heterogeneous rock salt provided microstructural evidence supporting hypothesis 1 and 3: permeation along the micro-cracked matrix halite grain boundary network and along the interface of matrix halite with halite mega-grains and/or anhydrite bands. The contribution of dissolution-precipitation was found to be of minor importance in this process. Pronounced hydrofracturing of intact halite grains, as posited by hypothesis 2, was not observed in the tests. Therefore, the extent of permeation along transgranular cracks could not be fully evaluated in this study. However, it is believed that transgranular cracks within halite mega-grains contribute to permeation, albeit to a lesser extent compared to permeation along phase interfaces and the present dilated grain boundaries. Permeation through porous anhydrite (hypothesis 4) was observed in the tested core pieces. However, it is thought to be related to experimental artifacts, particularly the preferential dissolution of associated polyhalite. This phenomenon is unlikely to scale with the conditions found in natural salt formations.

Interpreting the results presents challenges due to the heterogeneous behaviour of the samples and the limited quantity available. Across all samples, there is minimal segmented fracture space evident before permeation, and nearly no fracture space observed after permeation. Overall, all samples indicate low connected micro-porosity and consequently, a correspondingly low permeability of in-situ Zuidwending halite.

While further testing is required to better understand permeation behaviour and its relation to effective stress, the combination of microstructural investigations with laboratory testing proved to be a valuable addition. Microstructural evidence provides a better delineation of the microscale processes of permeation in heterogeneous rock salt and may help in future to categorically evaluate the permeation behaviour based on the microstructure.

References

Schenk O, Urai J; 2004. Microstructural evolution and grain boundary structure during static recrystallization in synthetic polycrystals of sodium chloride containing saturated brine. Contrib Mineral Petrol, 146:671-682.

Schmatz et al., in press, The Dutch Ministry of Economic Affairs, Knowledge Programme on Effects of Mining – KEM-28